DESIGN OF IONIZATION CHAMBERS FOR USE IN TEACHING X-RAY DOSIMETRY

By

Joseph Ross

Bachelor of Science in Medical Physics

East Central University

Ada, Oklahoma

2009

Submitted to the Faculty of the
Graduate College of the
Oklahoma State University
in partial fulfillment of
the requirements for
the Degree of
MASTER OF SCIENCE
July, 2015

DESIGN OF IONIZATION CHAMBERS FOR USE IN

TEACHING X-RAY DOSIMETRY

Thesis Approved:

Dr. Eric Benton

Thesis Adviser

Dr. David Peakheart

Dr. Eduardo Yukihara

ACKNOWLEDGEMENTS

I would like to thank my advisor Dr. Eric Benton for his continued insight and support. I would also like to thank my committee members Dr. Eduardo Yukihara and Dr. David Peakheart for their time and efforts with this project. And I would like to thank all of my colleagues in Dr. Benton's research group, past and present. And a special thanks to Art and Barbra Lucas for everything they have taught me.

I would also like to thank my wife Allison for her love, support, and patients.

Name: Joseph Ross

Date of Degree: JULY, 2015

Title of Study: DESIGN OF IONIZATION CHAMBERS FOR USE IN TEACHING X-RAY DOSIMETRY

Major Field: PHYSICS

Abstract: Ionization chambers are one of the most commonly used radiation detectors in radiation dosimetry. In this project, nine ionization chambers were constructed for use in teaching radiation dosimetry to students of health physics, medical physics, nuclear engineering, and related disciplines. The components of these detectors such as detector wall composition, type of electrode, type of leakage current guard ring, fill gas pressure, and interior conducting material differ in a systematic way to show that various parameters of ionization chamber design can affect the response of the detectors. Each of these variables was investigated using an 80 keV x-ray machine to determine detector response in terms of absorbed dose, HVL, polarity, and operating voltage. Of the components studied, wall thickness and composition was found to be the most sensitive variable. The pressure inside the chamber did have a significant effect on the amount of charge collected and the absorbed dose. The leakage current guard ring was not a critical component for this ionization chamber design.

TABLE OF CONTENTS

Chapter Page

LIST OF TABLES

Table Page

Table Page

LIST OF FIGURES

Figure Page

Figure Page

CHAPTER I

INTRODUCTION

The ionization chamber has been one of the most commonly used radiation detectors for over a century in the field of radiation dosimetry. There are several reasons that ionization chambers have continued to be a mainstay amidst all of the advances in technology. Ion chambers are amongst the simplest scientific instruments used for any high quality technical measurements. Employing no moving parts and generally having a composition of plastic polymers or aluminum, ionization chambers are robust and produce reliable results over long periods of time. Ion chambers can be easily constructed from low cost, readily available materials. Their simplicity also permits a wide variety of geometries, where different shapes and sizes are optimized for a wider range of applications.

One application of ionization chambers is as radiation survey instruments. They can be large or small volume chambers depending on what is being monitored. Smaller ion chambers are often used as portable radiation survey meters for environmental monitoring by health physicists. For occupational safety, large volume ion chambers are often placed around nuclear reactor

facilities and outside medical radiation rooms. This is especially important around nuclear medicine clinics to alert technicians of improper storage of radioactive sources.

Another application of very large ion chambers is in the calibration of radioactive isotopes. The radiation source can be placed directly inside of the ion chamber volume so that the activity of the source can be measured. Large volume ion chambers are generally used in situations where sensitivity to low intensity radiation is important. The large volume increases the probability that radiation will be detected and reduces the time required to obtain statistically significant data.

In a clinical setting, ionization chambers are used for automatic beam monitoring and also for quality assurance test of diagnostic and radiotherapy machines. Beam monitoring ionization chambers are designed to shut off radiotherapy machines when a predetermined dose is met or exceeded. A beam monitor may also be used with machines that use a linear accelerator to produce x-rays. Since the output of these machines is not always consistent, a beam monitor is used to normalize the measurements taken by other ion chambers. Quality assurance measurements are carried out using small Farmer or thimble type ion chambers. Their small volume is necessary for measuring narrow x-ray beams and for taking beam profile measurements. The small size is also important for the application of cavity theory when measuring depth dose curves in phantoms. It is necessary that the photoelectron fluence to be measured is not disturbed by the presence of the ion chamber. Throughout these different designs and applications of ion chambers, the basic principles of operation are the same.

Students preparing for careers in fields such as medical physics, health physics, radiation protection, and nuclear engineering need to have a firm understanding of how ionization chambers work and on how the various parameters of ionization chamber design can affect the response of the detectors. A good way for students to learn basic principles is through hands-on

teaching labs where students can use instruments and learn practical skills. Standard dosimetry classes teach students theoretical concepts, but it is important for students to actually quantify these differences with data to really get a sense of the significance. It is also important for students to see how using different ionization chambers to measure the same radiation source can produce different results, so they can learn why and how to make appropriate corrections. An example would be, by increasing the thickness of the ion chamber wall material, the apparent dose to the material would be underestimated because less gas is ionized inside the detector cavity, due to attenuation by the wall. Another practical example is the use of a beam monitor to correct for variations in x-ray beam intensity.

The objective of this thesis project was to design, fabricate, and characterize a number of ionization chambers capable of demonstrating some of the fundamental principles involved in radiation measurement and to investigate the difference in responses of detectors by varying certain parameters. Nine detectors were built with the same general dimensions, size and shape, but were constructed from various materials or with variations in the detector components. Some of the parameter variations include the wall material, use of leakage current guard ring, surface area of the electrode, interior conducting material, and air pressure in the cavity. All detectors were built in-house, at low cost, from readily available commercial plumbing hardware and salvaged electronics parts. The detectors were used to carry out investigations into absorbed dose, half value layer (HVL), operating voltage, and polarity effects. This thesis documents the design and results from these characterization experiments. I believe that these instruments can become the basis for a set of experiments for an introductory radiation dosimetry course.

CHAPTER II

BACKGROUND

Gas filled detectors can be used to measure all types of ionizing radiation, and there are many different ion chamber geometries and configurations. The same basic principles of operation apply to all gas filled detectors including ionization chambers, a class of gas filled detector characterized by the DC voltage range in which they are operated. This will be discussed in detail in Section 2.2.

Ion chambers operate by measuring the charge created when ionizing radiation passes through a gas. They consist of two electrodes to which an electric potential is applied, creating an electric field. When the gas between the electrodes is ionized by radiation, the charged ions are accelerated towards the electrodes. This motion of ions induces a current on the electrodes which can be measured by a sensitive ammeter called an electrometer. Figure 2.1 shows a diagram of the cross section of a cylindrical ion chamber that shows ion pairs liberated by ionizing radiation being attracted, under the influence of the electric field, towards the central electrode (anode) and the conducting cavity wall (cathode).

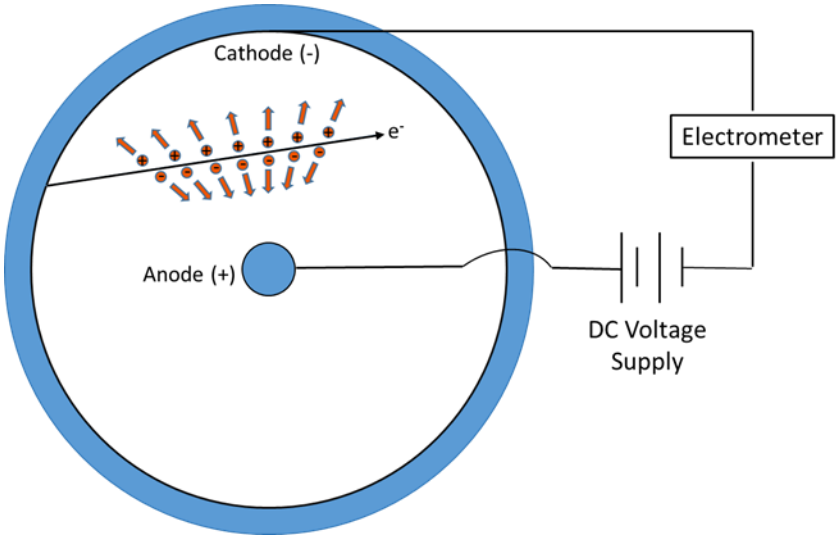

Figure 2.1 - Diagram of the cross section of a cylindrical ion chamber that shows ion pairs liberated by ionizing radiation being attracted, under the influence of the electric field, towards the central electrode (anode) and the conducting cavity wall (cathode).

For the cylindrical ion chambers constructed for this project, incident photons from the x-ray source interact with the wall of the detector or the gas inside the detector. Theoretically, monoenergetic photons do not have a finite range but are instead absorbed exponentially as a function of depth when passing through matter. The number of photons transmitted, N, through some material of thickness x, can be described by equation 2.1:

$$N(x) = N_0\, e^{-\mu x}, \tag{2.1}$$

where N_0 is the number of photons incident on the attenuating material and μ is the linear attenuation coefficient of the material or the "fraction of photons that interact per unit thickness of attenuator." [1] This equation may be used to calculate the attenuation by any thickness of material.

There are three main ways that a photon can interact with matter, the photoelectric effect, Compton scattering, and pair production. Since the x-rays used for the following experiments have energy less than or equal to 80 keV, the predominant interaction that will be considered is

the photoelectric effect. During the process of photoelectric effect, an incident photon is completely absorbed by an atom or molecule and an energetic secondary electron, with energy equal to the energy of the incident photon minus the electron binding energy, is ejected. The energetic secondary electrons primarily lose energy through collisions with atomic electrons as they pass through matter. Most collisions with atomic electrons lead to ionization, the liberation of an electron from the host atom, and excitation, the raising of atomic electrons to higher energy levels. The total number of ion pairs, created along the track of ionization in the gas, is the practical quantity of interest which is indirectly measured by ion chambers.

The charged ions created as ionizing radiation passes through the volume of gas are affected by the force of the electric field, F = qE, where q is the charge of the ions, created by the potential difference of the electrodes. The most common electrode configurations consist of positive and negative parallel plates or cylindrical ion chambers with a central electrode and an electrically conducting interior wall. In the cylindrical ion chamber design constructed for this project, the negative ions are attracted to the central electrode (anode) and the positive ions are attracted to the wall of the detector (cathode), as illustrated in Figure 2.1. Air is the most common fill gas in ionization chambers and it has a high electron attachment coefficient which means that the free electrons quickly attach to neutral molecules and negative ions are readily formed. [2] When the two electrodes of an ionization chamber are held at some electric potential difference, and the detector is subjected to some ionizing radiation, the flow of the ions created in the gas constitutes an electric current, the *ionization current*. The measurement of this ionization current is the basic principle of the dc ion chamber. [2]

If an ion chamber is originally charged to a voltage V_0, under ideal conditions, this voltage should be maintained indefinitely in the absence of ionizing radiation. When exposed to radiation, the ions created will act to partially discharge the capacitance of the ion chamber and reduce the voltage from its original value. The total charge stored on the capacitance will be

reduced by ΔQ, the charge created by ionization. By noting the voltage drop, ΔV, across the capacitance,

$$\Delta V = \frac{\Delta Q}{C}, \tag{2.2}$$

the total ionization charge or integrated ionization current over that period of measurement, can be deduced. [2]

If all of the ions created in the gas are collected by the central electrode and measured by the electrometer, the amount of energy deposited in the gas can be deduced. The average energy lost by the incident electron in the air is approximately 34 eV per ion pair created. This quantity is commonly referred to as the W-value and its exact value varies slightly in different sources of literature. [2, 3] For the calculations carried out in this thesis, the value 33.97 J/C was used. Using the w-value, the mass of air in the ion chamber cavity, m, and the total charge collected, Q, one can calculate the absorbed dose to air.

The absorbed dose is the amount of energy absorbed per unit mass. It is the quantity of most interest in radiotherapy and radiobiology. For the experiments performed with the constructed ion chambers, the absorbed dose to air, D_{air}, was the quantity used to compare the responses of the different detectors and is given by Equation 2.3:

$$D_{air} = \frac{Q}{m} * W. \tag{2.3}$$

Using the charge measured by the electrometer in Coulombs and the mass of air in kg, and the w-value in J/C, the SI unit of absorbed dose is the gray, abbreviated Gy. It is important to correct the mass of air for temperature and pressure using the Ideal Gas Law,

$$\rho_{air} = \frac{P}{R\,T}, \tag{2.4}$$

where ρ_{air} is the density of air, P is the air pressure, R is the ideal gas constant for air, and T is temperature. Then the mass of air is

$$mass_{air} = \rho\, V, \tag{2.5}$$

where V is the volume of the air cavity.

2.1 Factors Affecting the Measurement of Ionization Current

2.1.1 Saturation Current

One factor that can lead to the improper measurement of the ionization produced inside an ion chamber is ion recombination. In the absence of an electric field, the ions created by ionizing radiation would quickly recombine with the opposite species neutralizing the pair. The applied voltage to an ion chamber must be great enough to separate the ions quickly to ensure that all of the ions that are created by the radiation are collected. When all of the ions created are successfully collected and recombination is minimized, saturation current is achieved. The voltage range at which an ion chamber should be operated to achieve saturation is shown as Region II in Figure 2.2. Region II is known as the ionization region for gas filled detectors. In this region, the electronic output signal remains constant through a range of applied voltages. If the voltage is increased significantly beyond saturation, the accelerated ion can gain enough energy to produce more ionization. For a full description of the operating voltages for gas filled detectors, see Tsoulfanidis. [4] In the case of densely ionizing radiation or high intensity fields, the concentrations of ions becomes greater so the likelihood of opposite ions bumping into each other is increased. Therefore, a greater applied voltage is required to minimize the effects of ion recombination. In reference to Figure 2.2, V_1 increases. Region I indicates the region where ion saturation has not been achieved and complete ion collection does not take place. Other factors

such as humidity and ion chamber volume (i.e. the distance an ion must travel to be collected) affect ion recombination.

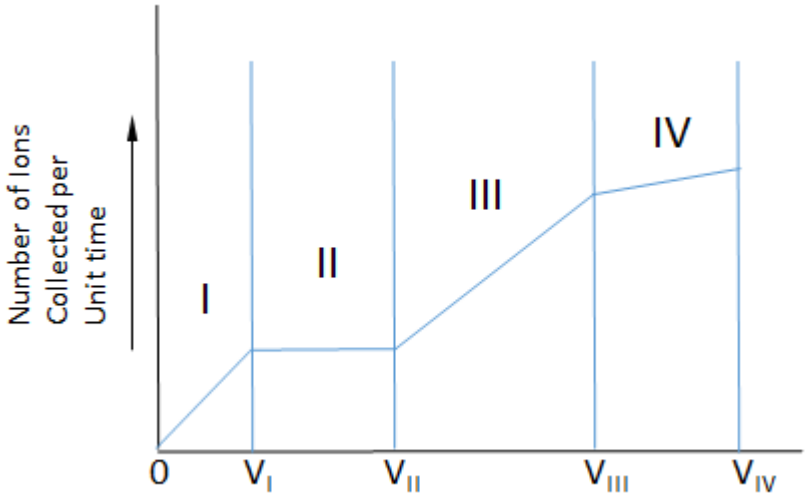

Figure 2.2 - Relationship between operating voltage and charge collection for the categories of gas filled detectors. Ionization chambers operate in Region II. [4]

2.2.2 Leakage Current

The two electrodes of an ionization chamber are typically separated by some sort of insulating material. Since, the charge typically measured by an ion chamber is of the order of pico or nano Coulombs, any current that leaks across the insulator can contaminate the signal significantly. Materials such as PVC have high resistivity, but moisture and contaminants can reduce the resistivity. When constructing an ion chamber, it is important to maintain a clean insulating surface.

In order to prevent or reduce the effects of leakage current, most commercial ionization chambers employ a leakage current guard ring. The guard ring is best depicted by the illustration from Knoll [2], in Figure 2.3. The guard ring is positioned between the insulating ring surrounding the

central electrode and another insulating ring separating it from the conducting wall of the detector. The leakage ring is connected the ground potential so that any leakage current will not contribute to the signal being measured.

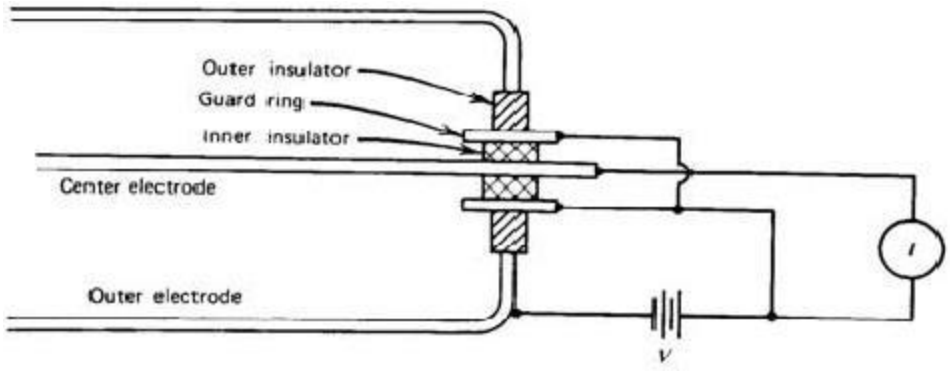

Figure 2.3 - "Cross sectional view of one end of a cylindrical ion chamber that utilizes guard ring construction. Most of the applied voltage V appears across the outer insulator, for which the resulting leakage current does not contribute to the measured current I." [2]

CHAPTER III

METHODOLOGY

3.1 Characterization of the El Vacatron X-ray Machine

The experiments to characterize the various ionization chambers constructed for this project were all carried out using the custom built El Vacatron 3000 x-ray machine. The El Vacatron is a one cubic meter wooden box lined with lead shielding. A Toshiba Model 100SS, 80 kVp MinXRay source, is contained in a separate housing attached to the outside of the box with the beam directed into the box through a hole centered in one of the walls. On the interior of the box, the beam is collimated using a wood-framed lead collimator with a one inch hole centered in line with the x-ray tube window. Because the El Vacatron is custom built, its performance needed to be characterized so that its operation would not interfere with the results obtained in comparisons of the various ion chambers.

Two ionization chambers and two electrometers, with calibration traceable to national standards laboratories, were used to characterize the El Vacatron x-ray system. The ionization chambers used were both PTW-Freiburg, models TN31014-000958 (PTW-958) and

TN30009-00781 (PTW-781). One electrometer was a Supermax Electrometer, S/N: P11292, made by Standard Imaging. The other electrometer was a PC Electrometer, reference S/N: 71230022, made by Sun Nuclear.

3.1.1 Interior Construction of the El Vacatron X-Ray System

In previous experiments using the El Vacatron system, significant inconsistencies in the amount of charge collected by ionization chambers were noted. The source of the inconsistencies could have been the x-ray beam, the ionization chambers, or slight variations in the position of the detectors in the beam. To address this issue before testing the detectors that were built in-house, the x-ray beam was characterized with two experiments.

Figure 3.1- Interior testing space of the El Vacatron x-ray system. To the left is the x-ray beam collimator and to the right is the ion chamber positioning stand and cross bar.

A rail system to position the detectors, pictured in Figure 3.1, was built inside the box, parallel to the axis of irradiation. Distances of 50, 60, and 70 centimeters were marked along each

of the two rails. A cross bar made to intersect the beam at the various distances was supported by the rails. The cross bar was marked and labeled in centimeter increments to give a relative lateral location in the cross section of the x-ray beam. A movable attachment to the cross bar was then made to hold the ionization chambers.

3.1.2 Changing Intensity

The two ionization chambers were used to measure the beam intensity as a function of position on the cross bar. Both ion chambers were attached to the cross bar slider about two centimeters apart. They were moved in unison through the marked positions on the cross bar. After the detectors were irradiated at all positions, the charge from both detectors was plotted together as a function of position. Through visual observation, the plots looked similar, but out of phase with each other. The same data was instead plotted as a function of successive irradiation. In the two plots, the amounts of charge measured by the detectors increased and decreased together for each irradiation. This indicated that the intensity of the x-ray beam was not consistent and that all future irradiations would need to be normalized by a stationary beam monitor.

3.1.3 Lateral Field Size

The lateral field size at different distances away from the x-ray tube window was determined. For each distance away from the tube window, the PTW-781 detector was placed on the cross bar and moved laterally through each marked position and irradiated while the second ion chamber, the PTW-958, used as the beam monitor, was held stationary between the x-ray tube window and the beam collimator. The beam monitor was placed at that location to prevent its presence from disturbing the beam while it was being measured along the cross bar. The ratio of the charge collected by the moving detector to the stationary detector was plotted as a function of lateral position along the cross bar. Three separate 30 second irradiations were measured for each

lateral position along the cross bar in both experiments. The outcome of these measurements is presented in the following chapter.

3.2 Ion Chamber Design

A total of nine ionization chambers were constructed for use in this project. All detectors were based on similar general design parameters and used air as the fill gas. Each detector consists of a cylinder, with an interior volume between 310 – 330 cm^3, with one exception. The exception has a smaller diameter, solid electrode resulting in a larger volume of air. One detector was sealed and pressurized; all others were operated at ambient temperature and pressure. The interior surface of the cylinder was made electrically conductive and connected to one lead of the high voltage power supply. The other lead of the power supply was grounded to a coaxial signal cable. A hollow aluminum electrode, secured in one of the endcaps, extended centrally through the cylinder and stopped approximately even with the distal end of the cylinder. The electrode was surrounded by an insulating ring that was also surrounded by a conductive guard ring which was grounded, to prevent leakage current. The ends of the cylinder were capped by a concave section of the same material used for the cylinder and were also made conductive. One cellular core PVC and one solid core PVC detector constructed adhere to these basic design parameters. The other PVC detectors are variations of the basic PVC design. One ABS plastic ion chamber and one aluminum ion chamber were compared with the basic models for comparison of the effect of ion chamber wall material. Although the aluminum ion chamber was not lined with graphite, it does employ the other basic design components.

As mentioned above, the effect of the choice of wall materials on the absorbed dose of the detector was the first design parameter to be investigated. Five modifications or variations on the basic design were also investigated. PVC is cheap and easy to machine so it was chosen as the basic material to construct the variations. Three variations of the solid core PVC basic model

were constructed and two variations of the cellular core PVC basic model were constructed. The general design of the basic PVC ionization chamber is illustrated in Figure 3.2.

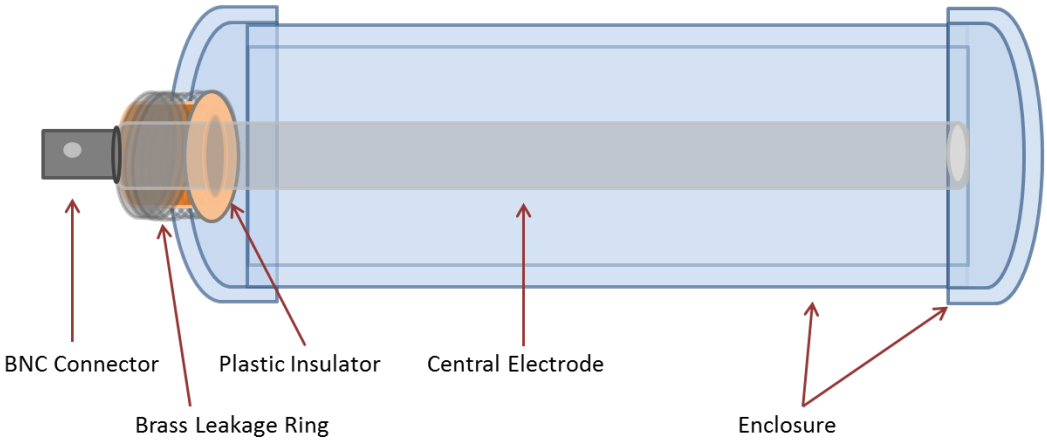

Figure 3.2– Diagram of the basic ionization chamber design.

One of the standards in commercial ionization chamber design is the three terminal design. Since very small currents are measured in dosimetry, any leakage current from the wall of the detector to the collecting electrode can contaminate the signal significantly. Since PVC is a good insulator and the size of the detectors is quite large, two detectors were constructed to determine the importance of the leakage current guard ring in this application. A cellular core PVC detector was constructed with a greatly reduced, superficial, guard ring (CPVC-R) and a solid core PVC detector was constructed with no guard ring at all (SPVC-NR). The specifics of these two detectors are described in the Ion Chamber Construction section. All of the ion chambers that were constructed were of the three-terminal design except the SPVC-NR.

The other variation of the cellular core PVC basic design was built to determine the effect of using a different conducting material on the interior walls of the detector. Graphite coating is commonly used in the construction of ionization chambers to make the inner walls conductive, but graphite is not as electrically conductive as aluminum. An ion chamber connected to an

electrometer acts like an RC circuit, where the ion chamber acts like a capacitor. When ionization current is present between the electrodes, there is a voltage drop across the capacitor. This voltage drop is proportional to the amount of charge collected. If one of the electrodes doesn't conduct as well as the other, then there may be some extra resistance on the circuit. By changing the conducting surface to aluminum, the resistance may be reduced and there may be a noticeable difference in the amount of charge measured. One ion chamber, CPVC-Al, was constructed with a single layer of aluminum foil lining the interior of the wall to determine if the increased conductivity had any effect on detector response.

Another variation that was used to determine the effect on collection efficiency was the use of a different central electrode design. The large hollow central electrode of the solid core PVC basic detector was exchanged for a solid, slender aluminum electrode that had a much smaller surface area for collection than did the basic model (SPVC-SE).

The final variation of the solid core PVC basic design was a pressurized detector (SPVC-P). It was constructed using all of the basic design parameters but it was sealed and pressurized to measure the effects of increased pressure and mass of air inside the chamber on the absorbed dose measured by the detector.

The specifications for all of the detectors are described in the Ion Chamber Construction section of this thesis. The dimensions of the different types of ion chambers were not exactly the same due to differences in the dimensions of building materials used, such as interior pipe radii and types of endcaps that were available. An effort was made to make the volumes of gas inside the detectors as similar as possible by varying the length of the detectors slightly.

3.3 Ion Chamber Construction

Four different wall or gas enclosure materials were used in the construction of the ionization chambers. They included solid core PVC (schedule 40), cellular core PVC (schedule

40), cellular core ABS (schedule 40), and aluminum pipe (schedule 10). See Table 3.1 for density of materials, average wall thickness, chamber volumes and masses of air. The chamber volumes were measured by determining the mass of water needed to fill the detectors minus the volume of water displaced by the electrode assembly. The density of wall material was also measured using the water displacement method.

Table 3.1 - Physical specifications of the 9 detectors built in EVB Radiation Physics Laboratory. Mass of air listed for SPVC-P was with detector pressurized to 2 atm. The other masses used during measurement with 3 atm and 4 atm were .000794 kg and .00119 kg, respectively.

Ionization Chamber	Wall Density (g cm^{-3})	Average Wall Thickness (cm)	Overall Length (cm)	Interior Volume (cm^3)	Mass of Air (kg)
ABS	.715	.41	15.5	325	.000376
CPVC-B	1.08	.44	17.5	310	.000385
CPVC-R	1.08	.44	17.5	310	.000362
CPVC-Al	*	*	17.5	331	.000412
SPVC-B	1.45	.42	17.5	319	.000374
SPVC-NR	1.45	.42	17.5	329	.000394
SPVC-SE	1.45	.42	17.5	342	.000411
SPVC-P	1.45	.42	17.5	325	.000397
Aluminum	2.7	.26	15.25	320	.000381

3.3.1 Solid Core PVC Ion Chambers

The body section of the first three detectors was constructed from 2" schedule 40, solid core PVC pipe. The cylindrical pipe was cut into 14 cm long sections using a band saw. Both of the ionization chamber end caps were standard schedule 40 PVC pipe caps. A lathe was used to modify one end cap and remove about 2 cm from the lip so that only about 1.5 cm of cap would overlap the cylinder walls. The center of this cap was also removed using the lathe and a smaller hole was drilled off center with a drill press. A central electrode and high voltage power supply wire were passed into the interior where the wire was secured to the interior wall of the cylinder with silver conducting epoxy. In order to make the interior walls of the chamber electrically conductive, the interior surfaces of the chamber volume were coated with an aerosol graphite

spray, Aerodag G, except for a small uncoated ring surrounding the electrode entrance area of the cap. This insulating ring of uncoated PVC is present to help prevent leakage current. The other end cap was also turned on the lathe to remove all but 0.5 cm from the lip. No other modifications were made to the PVC shell.

Figure 3.3 – (Left) Hardware used to construct the basic electrode assembly of the SPVC-B ion chamber. (Right) The finished electrode assembly seated in the graphite coated PVC endcap.

The electrode assembly, pictured in Figure 3.3, was made from modified plumbing hardware and scrap aluminum tubing. The ½" aluminum tubing was cut to 16.5 cm length and a male BNC connector was secured to the interior of the central electrode. The charge collected on the electrode is sent to an electrometer via a coaxial cable.

The signal from the electrode needs to be protected from leakage current from the conducting wall of the detector, so a series of rings were arranged around the electrode. An insulating ring of plastic made from a PVC male adapter was turned on the lathe and trimmed on the band saw to fit into the next modified piece of plumbing hardware. A brass guard ring connected to electrical ground completely surrounded the insulating ring and was used to carry away any charge that may have crossed the bare PVC insulating region. The guard ring was made from a ¾" brass fitting, which was then cut in half. The completed solid core PVC basic detector

(SPVC-B) is shown in Figure 3.4. Three more detectors of the solid core PVC design were constructed**,** each with one component variation.

Figure 3.4 - The solid core PVC basic ion chamber (SPVC-B). The interior wall was coated with graphite to make it conductive.

In order to quantify the importance of the guard ring used to prevent leakage current, a detector was built with the same specifications as the SPVC-B, except that the leakage current guard ring was removed. The electrode was surrounded by the PVC adapter for extra insulation and then secured into the PVC endcap with epoxy, pictured in Figure 3.5. There was also a ring of bare PVC around the PVC adapter to separate the graphite coated region from the electrode assembly. This detector is referred to as (SPVC-NR).

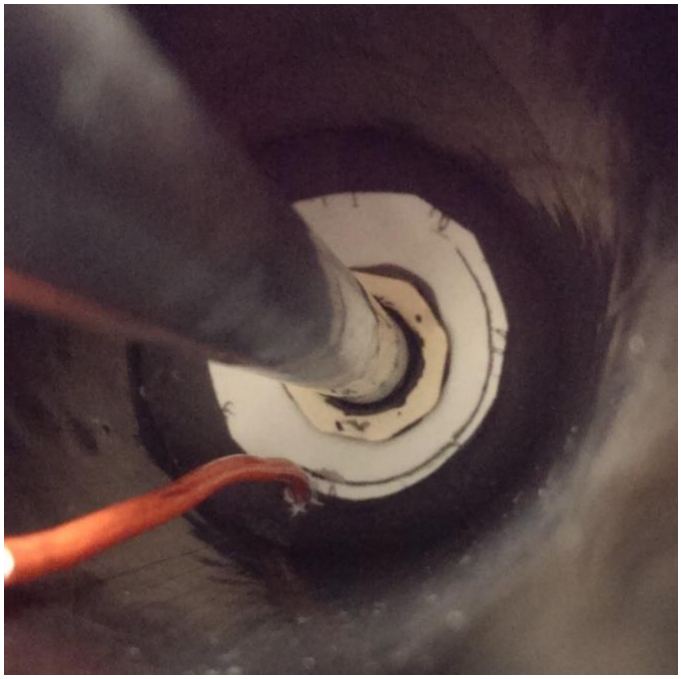

Figure 3.5 - The electrode assembly of the solid core PVC ion chamber without a leakage current guard ring (SPVC-NR) was placed directly into the endcap.

Another variation of solid core PVC basic ion chamber, referred to as SPVC-SE, used a solid, more slender aluminum rod to replace the basic hollow electrode that has a much larger surface area. A thin plastic ring was used to support the distal end of the electrode for increased stability. A ¼" aluminum rod was cut to about 17 cm in length so that it would reach approximately the same depth inside the chamber as the basic model's electrode. An HV connecter was modified and used as a base to connect the electrode to the male BNC connecter. Once again the electrode was fitted inside the basic insulating ring and brass guard ring. The electrode assembly of the SCPVC-SE detector is shown in Figure 3.6 and 3.7.

Figure 3.6 – Some of the electrode assembly components and the finished product of the SPVC-SE ion chamber.

Figure 3.7 – The HV connecter and the BNC connecter were used to construct a solid base for the SPVC-SE electrode.

The final variation of the solid core PVC basic design was a pressurized ionization chamber. It was constructed to demonstrate how changing the mass of air inside the chamber would affect the amount of charge collected and consequently the absorbed dose. A small hole

was drilled into the PVC endcap to mount a 1/8" Schrader valve and pressure gauge. In an effort to make the detector completely air tight, PVC cement, silicone, epoxy, super glue, and Teflon thread tape were used at various component junctions. The SPVC-P ion chamber was pressurized to approximately 2, 3, and 4 atmospheres, absolute pressure. The pressurized PVC detector (SPVC-P) is shown in Figure 3.8.

Figure 3.8 – The pressurized solid core PVC detector (SPVC-P).

3.3.2 Cellular Core PVC Ion Chambers

One detectors was constructed using all of the same design parameters as the solid core PVC basic, but constructed from cellular core PVC, the CPVC-B. There were two variations from the CPVC-B design.

In the first variation (CPVC-R), the basic electrode assembly was simplified and replaced by a superficial guard ring and the electrode was placed directly through the PVC endcap without extra insulation. Instead of the guard ring penetrating the endcap, the center of a large flat metal washer was removed and the remaining ring was seated into a scored ring on the inner surface of the endcap. A wire was soldered to the ring and run through a small hole drilled through the ring

seat. The washer was secured into place with silicone. A small insulating region was left on both sides of the guard ring to minimize leakage current. The electrode fit tightly into the hole drilled through the endcap and was secured into place with epoxy. Figure 3.9 shows the superficial guard ring.

Figure 3.9 – Shows the superficial guard ring of the CPVC-R detector, used in place of the brass cylinder guard ring.

For the final variation of the cellular core PVC detectors (CPVC-Al), only the conducting medium was changed from the CPVC-B design. A single layer of aluminum foil was used to line the interior surface of the detector instead of the graphite. The aluminum foil is a better conductor than graphite so it was thought that the detector may respond differently when collecting charge due to less resistance on the circuit. The CPVC-Al detector is shown in Figure 3.10.

Figure 3.10 – The cellular core PVC detector lined with aluminum foil (CPVC-Al).

3.3.3 ABS Ion Chamber

Only one detector (ABS) was made from 2" cellular core ABS pipe. The electrode assembly remained the same as the basic PVC designs above and the interior surface was coated with graphite. The ABS endcaps available for purchase do not come in a concave shape like that of the PVC caps. In an attempt to maintain design consistency through all the detectors, one ABS endcap was heated and worked into a somewhat concave shape. Due to difficulty in doing so symmetrically, and the need for the electrode to be as symmetrically axial as possible, the base endcap was not modified in this way. However, both endcaps' lips were trimmed to reduce the amount of overlap of the ABS cylinder. The cylinder length was approximately 13.8 cm and the electrode was shortened to 15.5 cm. The completed ABS detector is shown in Figure 3.11.

Figure 3.11 – The completed ABS detector.

3.3.4 Solid Aluminum Ion Chamber

A solid aluminum detector was built using schedule 10 pipe and two aluminum endcaps. One endcap was an aluminum hemisphere, cut on the lathe and then ground down to fit appropriately on the end of the pipe where it was secured into place using silver conducting epoxy. The endcap used to house the electrode assembly was a thread protector cap which overlapped the cylinder approximately 1.5 cm. The electrode assembly for this detector, pictured in Figure 3.12, was somewhat unique. It featured the basic electrode assembly with a brass leakage ring but since the endcap was made of metal, another insulating ring of PVC was used to separate the two. The plastic ring was a larger PVC male adapter epoxied into place. The aluminum pipe had an approximately 5.5 cm inside diameter so the cylinder length was shortened to 13.5 cm so that the interior volume would be more comparable to the PVC detectors. The shorter cylinder required a shorter 14 cm electrode. The completed aluminum ion chamber is pictured in Figure 3.13.

Figure 3.12 – (Left) The insulated electrode assembly used in the aluminum ion chamber. (Right) Exterior of the electrode assembly.

Figure 3.13 – The completed aluminum ion chamber.

3.4 Experimental Method

3.4.1 Experimental Setup

For each irradiation, the ion chamber was centered in the x-ray beam between the 6 cm and 23 cm markers on the cross bar at a distance of 70 cm from the x-ray tube window using the rail system discussed in Section 3.1. The PTW-958 ion chamber was used as the beam monitor and placed between the x-ray tube window and the beam collimator as described in Section 3.1.

The experimental detectors and the PTW-958 were connected to separate electrometers throughout the data collection process.

For each detector, the signal from the charge collected on the electrode is conveyed via a BNC connecter at the end of the central electrode and through a coaxial cable to the electrometer. The coaxial cable was attached via coaxial/triaxial converter to the triaxial input of the Sun Nuclear electrometer. One advantage of the Sun Nuclear electrometer is that it is capable of producing a data spreadsheet that records charge collected every half second, so the total charge collected by each of the ion chambers can be extrapolated to a set amount of time more accurately.

The high voltage was applied to the detectors using an ArmaLab 800 V external power supply. The negative lead of the power supply was applied to the interior wall of the detectors, while the positive lead was grounded to the coaxial cable connector and leakage ring. The electrometer also has its own power supply meant for use with commercial ionization chambers and triaxial cable, but it was set to 0 V so that the electrode of the experimental detectors will collect negative ions.

The PTW-958 was connected to the Standard Imaging electrometer with a triaxial cable and was powered by the electrometer's built in power supply. The electrometer power supply was set to +400 V as suggested on the PTW-958 calibration certificate. This electrometer displayed the total charge collected over the predetermined time setting but did not produce a time specific spreadsheet.

3.4.2 Procedure

Each detector was subjected to the same series of measurements in order to make possible a comparison of detector response. The general goal was to compare the cellular core PVC, solid core PVC, ABS, and aluminum models based on the material used to build each

detector, but also to analyze how the component variations of the cellular core and solid core PVC designs effect the performance of the detectors. The response of each detector was analyzed using four main points of comparison: 1) absorbed dose to air, 2) half value layer (HVL), 3) polarity effects, and 4) operating voltage.

Due to the uncertainty of the cause of the beam inconsistency in the x-ray machine, a warm up period for the x-ray machine and electrometers was allowed to elapse before the recording of charge began for each trial. The beam was allowed to run for approximately 10 seconds before the electrometers were initiated. The electrometers recorded charge for 15 seconds, and the beam remained on for an additional 5 seconds to ensure there was no discrepancy between the beam shut off before the electrometer recording ended. In short, the beam was on for 30 seconds but the electrometers were only recording the charge collected by the ion chambers for 15 seconds. Each 30 second irradiation was followed by a one minute tube cool down. For each irradiation, both electrometers were manually initiated simultaneously.

Prior to irradiation, each detector was used to measure the background radiation inside the shielded El Vacatron x-ray machine. Background was measured ten consecutive times with no high voltage bias applied to the detector and then ten more times with a detector bias of +600 V. It was decided, based on preliminary data from the first detectors built, that a standard operating voltage bias of +600 V would be used for all measurements for consistency. However, an operating voltage test was conducted on each detector for comparison. Each detector was irradiated three times for each 50 V interval starting with a bias of +100 V extending to +750 V.

After background and operating voltage measurements were taken, the effect of bias polarity on charge collection efficiency was analyzed. Ten measurements were taken with the x-ray beam on and a detector bias of +600 V, followed by ten more measurements using an

operating voltage of -600 V. The charge collected using negative polarity to the wall of the detector was also used to calculate the absorbed dose to the gas.

Finally, the HVL of aluminum was measured with each detector. The detector was first irradiated with only the x-ray tube window attenuating the beam, this was considered I_0. Then, sheets of aluminum were placed on the distal side of the lead collimator to attenuate the beam. Three irradiations were made for each thickness of attenuator, including I_0 measurements. Thin sheets of bulk aluminum of various thicknesses were added for each successive attenuation setting. The charge collected was then plotted as a function of attenuator thickness. The plot was fit with an exponential decay function and the mass attenuation coefficient and HVL were obtained.

CHAPTER IV

RESULTS AND DISCUSSION

4.1 El Vacatron X-ray Machine

The lateral field size of the El Vacatron x-ray beam was measured by normalizing the charge collected by the moving ion chamber by the charge collected by the stationary ion chamber. This corrected for the variation in beam intensity. At a distance of 70 cm, the relative intensity of the collimated beam was very symmetric and centered in the interior volume of the El Vacatron. The area of most uniform intensity was only about 5 cm wide, much smaller than the length of the large ion chambers that were constructed. To maintain consistency in the relative beam intensity received by all of the ion chambers, the ion chambers were approximately centered between the 6 cm and 23 cm markers on the cross bar so that the detectors were centered in the beam.

The length of the detectors could affect the amount of charge liberated inside the gas because the relative intensity of the beam drops sharply towards the ends of the detectors. The aluminum ion chamber, the shortest, was over two centimeters shorter than the PVC ion

chambers, which are the longest. Figure 4.1 shows that a centimeter difference on both ends of the exposed volume could significantly change the beam intensity experienced by the detector. A direct comparison of two detectors constructed of the same materials, but of slightly different lengths, was not carried out.

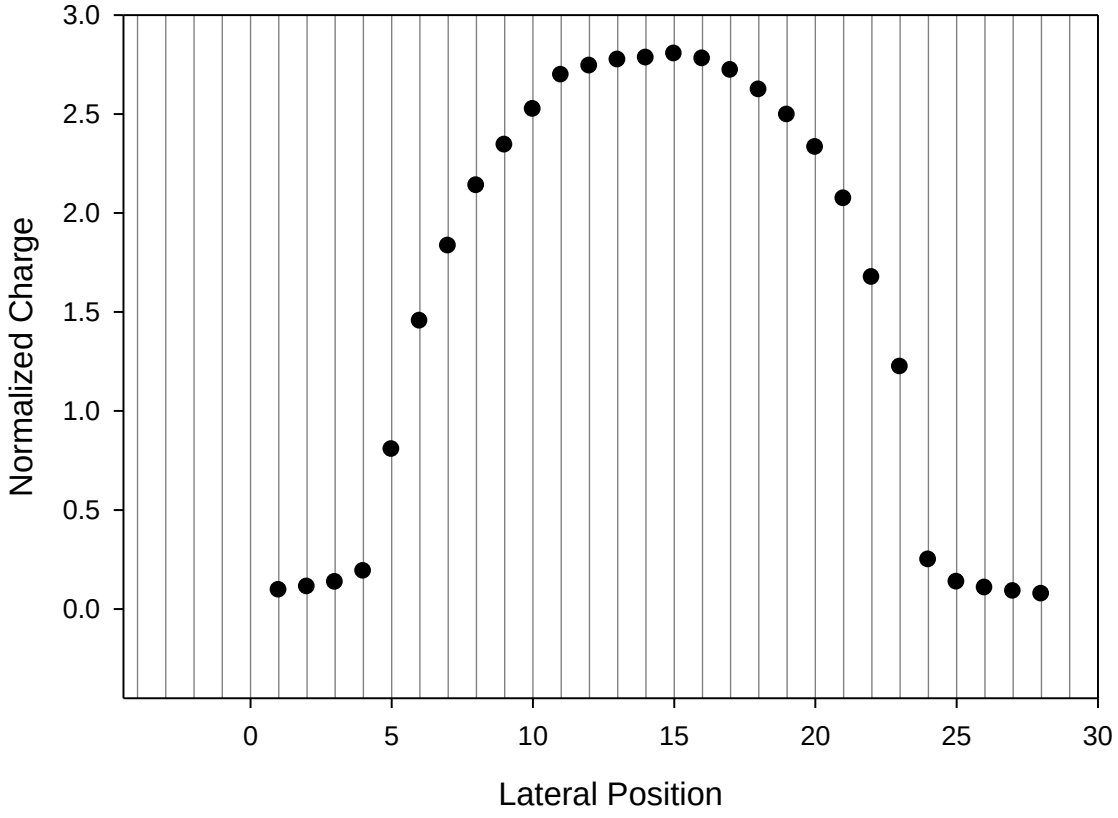

Figure 4.1 - Lateral Intensity of the beam inside the El Vacatron x-ray machine.

4.2 Data Analysis and Error

In all experiments, the charge collected by each ion chamber was normalized by the charge collected by the PTW-958. The PTW-958 was always connected to the standard imaging electrometer. Each of the other ion chambers was connected to the Sun Nuclear electrometer. The

data sheet produced by this electrometer was then used to extrapolate the amount of charge collected for exactly 15 seconds.

Charge was measured and the absorbed dose and HVL were calculated using the charge collected by the two ionization chambers. The error in the measurement of charge was determined as follows:

The normalized charge, q_1, is

$$q_1 = \frac{x_1}{w_1}, \tag{4.1}$$

where x_1 is the charge collected by the ion chamber, and w_1 is the charge collected by PTW-958. The uncertainty in q_1 is

$$\delta q_1 = q\sqrt{\left[\frac{\delta x_1}{x_1}\right]^2 + \left[\frac{\delta w_1}{w_1}\right]^2}, \tag{4.2}$$

where δx and δw are the smallest quantities measurable by the electrometers. In the case where more than one measurement was taken, the average uncertainty was

$$\overline{\delta q} = \frac{1}{n}\sqrt{\sum (\delta q_n)^2}, \tag{4.3}$$

where n is the number of measurements.

The uncertainty propagation in the dose calculations is slightly different than the uncertainty in charge. Due to the fact that the mass of air in each ion chamber was different from the mass of air in the PTW-958, the dose to each ion chamber was calculated separately. So the uncertainty in dose is the smallest quantity measurable by the electrometer times a constant that is proportional to the mass of air inside that particular chamber. Then the dose calculated for the experimental detector was normalized by the dose of the beam monitor. The uncertainty of the ratio of the two doses could then be calculated.

The best approximation for uncertainty in dose, δD, is the smallest quantity measurable by the electrometer used to measure the charge, 0.01 pC, times the constant $\left(\frac{w}{m}\right)$. The error in the ratio of doses, $r = \frac{D_1}{D_2}$, is

$$\delta r = r\sqrt{\left(\frac{\delta D_1}{D_1}\right)^2 + \left(\frac{\delta D_2}{D_2}\right)^2}. \tag{4.4}$$

Error bars were added to all plots shown, but the error calculated in most cases was so small that it only appeared as a line bisecting the symbols representing the data points.

4.3 Detector Response Comparisons

4.3.1 Ion Chamber Wall Material

4.3.1.1 Absorbed Dose in Air

The first experiment was to compare the absorbed dose in air measured by the four experimental detectors constructed from differing wall materials: ABS, cellular core PVC, solid core PVC, and aluminum. All of these detectors use the three terminal electrode design and have similar interior volumes coated with graphite, with the exception of the aluminum detector, which was not coated. The physical parameters of the wall material, listed in Table 4.1, that were used for comparison of the average normalized absorbed dose of each detector were areal density, electron density, and average atomic number divided by atomic weight ($\overline{Z}/A_w$).

Table 4.1 - Physical parameters of wall materials to be investigated and the absorbed dose measured by each detector normalized by the absorbed dose measured by the beam monitor.

Ionization Chamber	Wall Thickness (cm)	Areal Density (g/cm2)	Electron Areal Density (e^-/cm^2)	$\overline{Z}/A_w$	Average Normalized Dose
ABS	0.41	0.29	9.5E+22	5.83	0.0143
CPVC-B	0.44	0.48	1.5E+23	11.77	0.0126
SPVC-B	0.42	0.61	1.9E+23	12	0.0104
Aluminum	0.26	0.70	2.0E+23	13	0.0090

Charge was collected in ten consecutive trials for each ion chamber. The PTW-958 beam monitor was also irradiated during each trial. The mass of air inside each chamber, corrected for temperature and pressure, was used to calculate the dose in air for each chamber. The dose calculated for each detectors was then normalized by the dose calculated for the beam monitor for the same set of trials. Figure 4.2 shows the normalized absorbed dose of the four detectors.

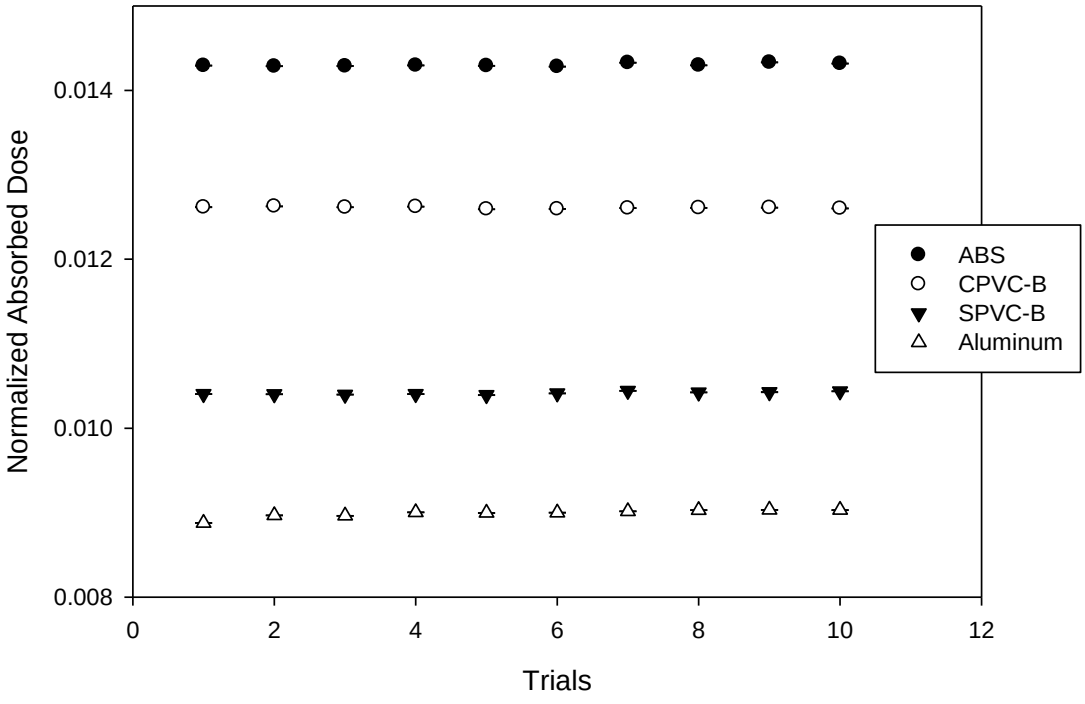

Figure 4.2 – The dose measured by each detector normalized by the dose measured by the beam monitor for the same trial.

There is greater than 10% difference between the normalized absorbed doses measured for each type of detector. The ion chambers appear to be ordered with the least dense, ABS, measuring the greatest dose, and the most dense, aluminum, measuring the least absorbed dose. This indicates that the aluminum wall is attenuating the beam more effectively than the ABS wall, therefore, less air is being ionized inside the aluminum detector, resulting in less charge being collected.

Consider the two main interactions that dominate in the photon energy range used during testing that take place in order to deposit energy in a standard ionization chamber, as illustrated in Figure 4.3. First, an incident photon can interact with the wall material producing secondary electrons that may then travel through the rest of the wall and into the cavity, depositing energy in the air. Or the incident photon can pass through the wall and interact directly with the air in the cavity, producing secondary electrons which travel through the air and also deposit energy in the cavity.

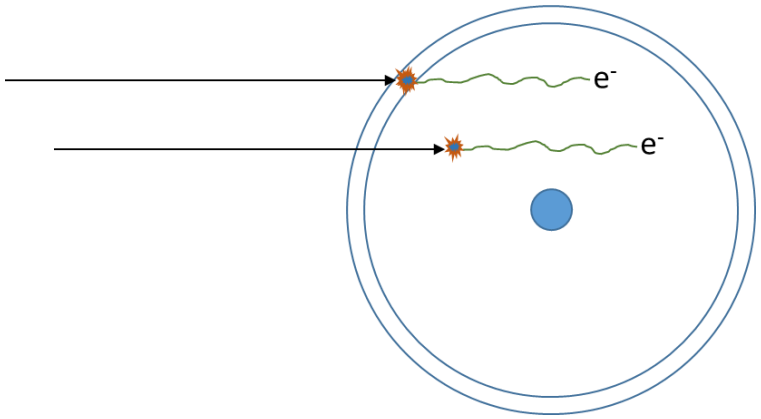

Figure 4.3 - Cross sectional view of a standard ionization chamber and the photon interactions. The upper arrow shows an interaction in the wall of the detector that creates a secondary electron that enters the cavity, while the lower arrow shows a photon interaction with the air in the cavity.

A thicker or denser wall will increase the probability of interactions in the wall reducing the amount of ionization inside the cavity in two ways. First, an electron produced in the wall will

have to continue through the rest of the wall and into the cavity to deposit its energy. The continuously slowing down approximation (CSDA) range of an 80 keV electron in solid core PVC is less than a millimeter.[5] Due to the thickness of the wall and the low energy of the electrons being liberated in the wall, many electrons produced in the wall will not make it into the interior volume to deposit their energy. Second, the increased probability of interaction with the wall reduces the intensity and probability of the x-ray beam interacting directly with the air inside the cavity. This two-fold effect would explain the decreased absorbed dose of the detectors with increased density as shown in Figure 4.2.

Based on these observations, an attempt was made to find a relationship between the density of the wall and the measured absorbed doses. The dose measured by each detector was calculated and normalized to the dose measured by the beam monitor for the corresponding trial. Since the ion chambers made from different materials have different wall thicknesses, the average normalized absorbed doses were plotted in Figure 4.4 as a function of areal density of the detector wall.

As shown in Figure 4.4, the linear fit of the data points indicates that there is in fact a strong correlation between the areal density of the wall and the dose absorbed by the air inside the cavity. Since, the detectors were tested on different days, sometimes several weeks apart, the less than perfect fit could be caused by humidity or minor detector placement variations in the beam. The differences in detector length affecting the photon energy spectrum incident on each detector could also affect the absorbed dose significantly.

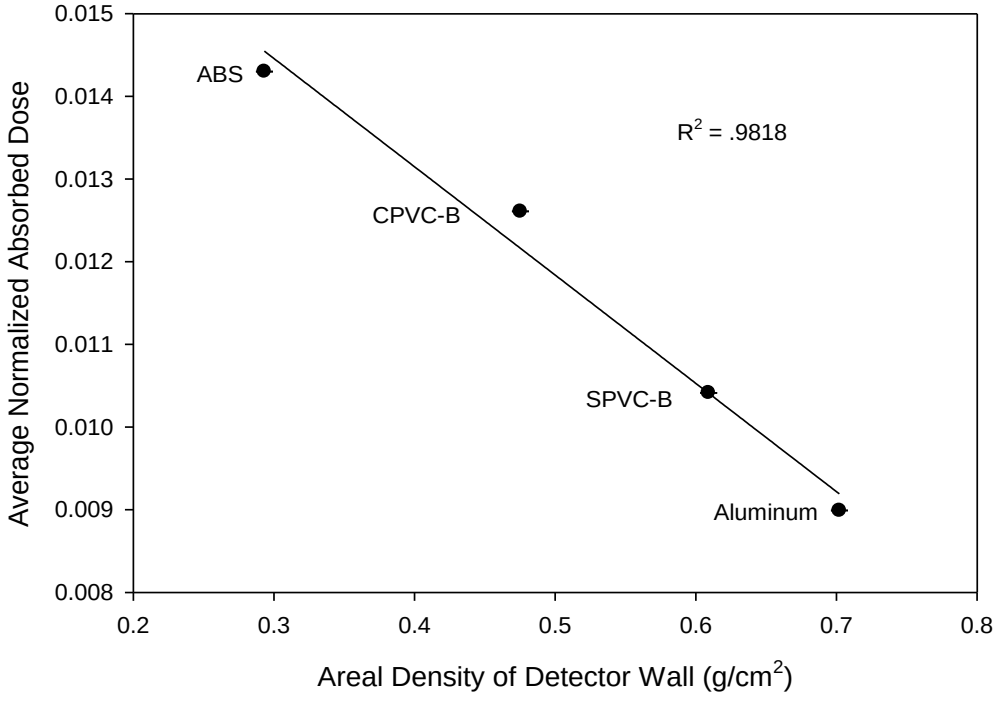

Figure 4.4 – Shows the absorbed dose measured by each detector normalized by the absorbed dose measured by the beam monitor, averaged and plotted as a function of the areal density of the detector wall.

Most of the detector walls are composed of mixtures of different elements, so it may be useful to describe the wall materials by the average atomic number, $\overline{Z}$. The average normalized absorbed doses were plotted again, but as a function of the average atomic number divided by the atomic weight ($\overline{Z}/A_w$) of each detector wall material. The average $\overline{Z}/A_w$ was determined from the chemical formula of the material. For example, the $\overline{Z}/A_w$ of PVC, ($C_2\ H_3\ Cl$), was determined as:

$$\overline{Z}/A_{w,PVC} = \frac{(2 * 6 * 12.01) + (3 * 1 * 1.01) + (1 * 17 * 35.45)}{(2 * 12.01 + 3 * 1.01 + 1 * 35.45)} = 12,$$

This determination seems reasonable, but ABS and cellular core PVC are less dense and appear to contain some air. An examination of the cross section of the pipes indicate that some

fraction of the composition is air bubbles. An estimate, based solely on the appearance of the cross section of pipe, was made to include the air content in them. The average $\overline{Z}/A_w$ of air was calculated to be 7.38 because it is roughly 78.1% Nitrogen, 20.9% Oxygen and less than 1% Argon by volume.

Based on ABS chemical composition $\overline{Z}/A_w$ was found to be 5.66, so if the ABS wall is considered to be 10% air,

$$\overline{Z}/A_{w\,ABS}\ with\ air = (5.66 * .9) + (7.38 * .1) = 5.83.$$

Similarly, cellular core PVC was estimated to contain 5% air. The $\overline{Z}/A_w$ of each building material is listed in Table 4.1. The thickness of the wall was also considered for each detector. The average normalized absorbed doses are plotted in Figure 4.5 as a function of $\overline{Z}/A_w$, corrected for air content, times the wall thickness.

It appears that there is no correlation between the $\overline{Z}/A_w$ of the detector wall material to the absorbed dose measured by the detector. The most notable observation in Figure 4.5 are the positions of the PVC detectors. Due to their very similar wall thickness, they are the most directly comparable. No chemical difference between the composition of cellular core PVC and solid core PVC was discovered during research. That would mean that the only difference between the compositions of the two kinds of detectors is the air content in the cellular core PVC. The possibility that the air content was under estimated was considered next. If the ABS detector and CPVC detector contain 40% and 30% air, respectively, then the average $\overline{Z}/A_w$ of ABS and CPVC changes by 8.5% and 10.3% respectively. In order to assess how the change in $\overline{Z}/A_w$ would affect the plot, the average normalized absorbed doses were plotted again using the recalculated $\overline{Z}/A_w$ times wall thickness, in Figure 4.6.

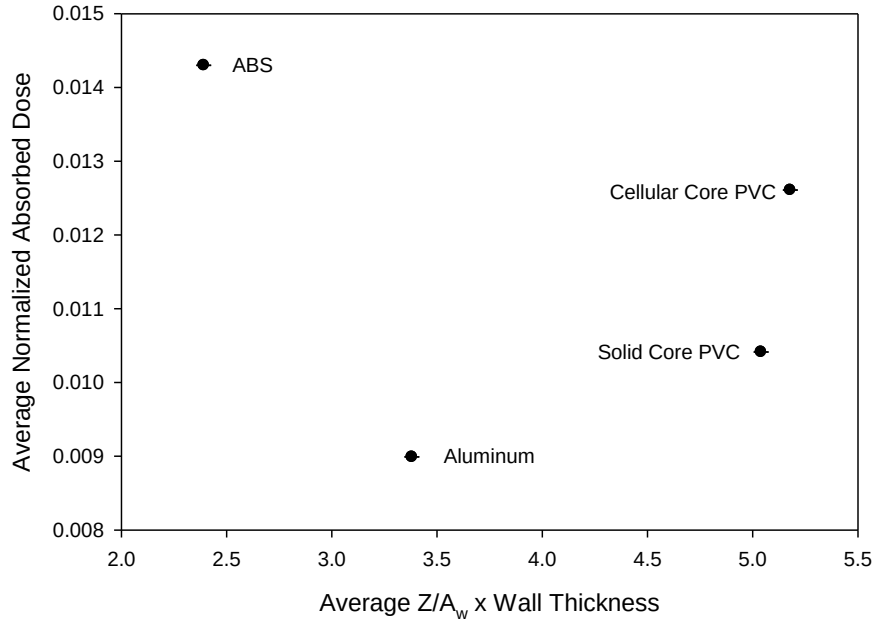

Figure 4.5 - The average normalized absorbed dose of each detector plotted as a function of $\overline{Z}/A_w$, corrected for air content, times the wall thickness.

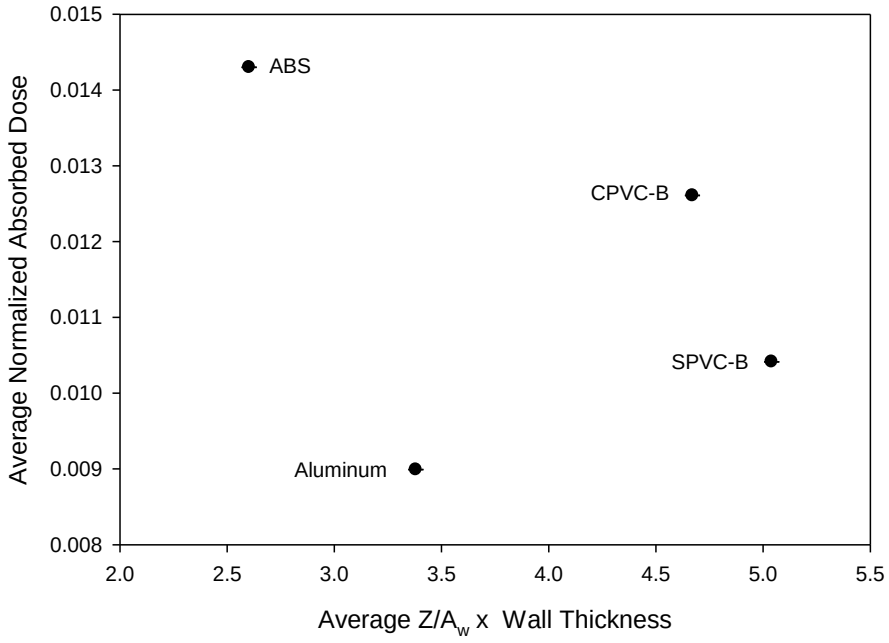

Figure 4.6 - The average normalized absorbed doses of each detector plotted as a function of $\overline{Z}/A_w$ recalculated with ABS considered to contain 40% air and CPVC to contain 30% air.

While there is better correlation between the detectors of similar wall thickness, this estimation of air content is assumed to be excessive based solely on visual inspection of the materials that were used. Although aluminum has the greatest average atomic number Z, the walls of the aluminum detector are much thinner than the walls of the other three, so this comparison is not entirely straightforward.

Continuing with the investigation of relationships between ion chamber composition and absorbed dose, electron density in the wall material was considered next. The electron density of each material was calculated using the chemical formula and Avogadro's number:

$$Contribution\ of\ Each\ Component = \frac{N_A * Z * \%\ by\ Weight}{A_w} = \frac{\#\ e^-}{g}.$$

The contributions from each element in the mixture were summed to obtain the total number of electrons per gram of material. This was then expanded in Figure 4.7 to include the density and thickness of the wall of the detector, giving electron areal density in units of $\frac{\#e^-}{cm^2}$.

The ABS and cellular core PVC wall materials were again considered to contain 10% and 5% air, respectively. The contribution of air to the overall electron density was calculated in the same manner that $\overline{Z}/A_w$ was calculated previously. Air contains about 3.01×10^{23} electrons per gram, making the adjusted electron density in ABS 9.45×10^{22} electrons per gram and 1.46×10^{23} electrons per gram in cellular core PVC. The normalized absorbed dose was then plotted in Figure 4.8 as a function of electron density, corrected for air content. The results of both plots, Figures 4.7 and 4.8, are very similar to Figure 4.5 and appear to be dominated by the areal density component of the calculation.

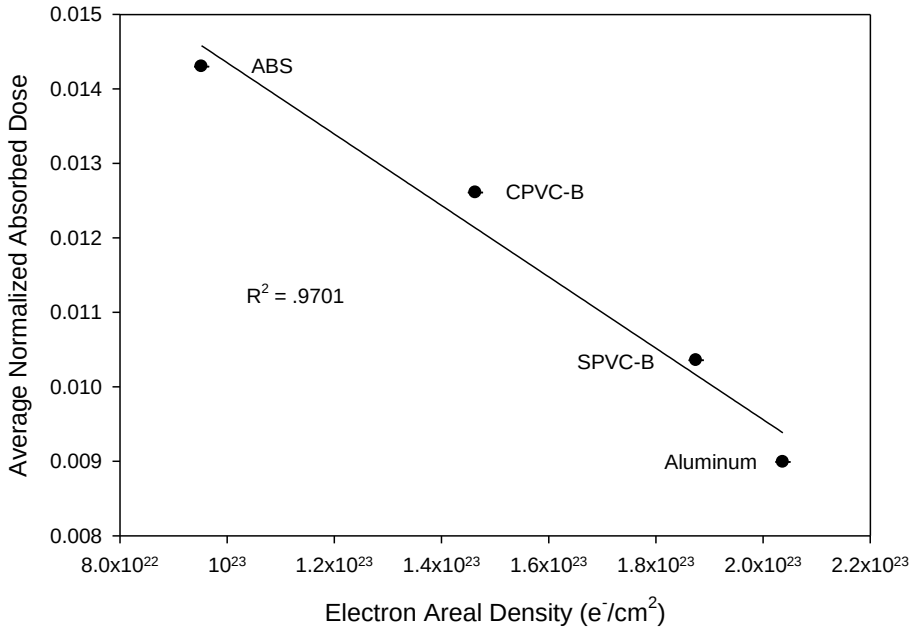

Figure 4.7 – Shows the absorbed dose measured by each detector normalized by the absorbed dose measured by the beam monitor, averaged and plotted as a function of the electron areal density of the detector wall.

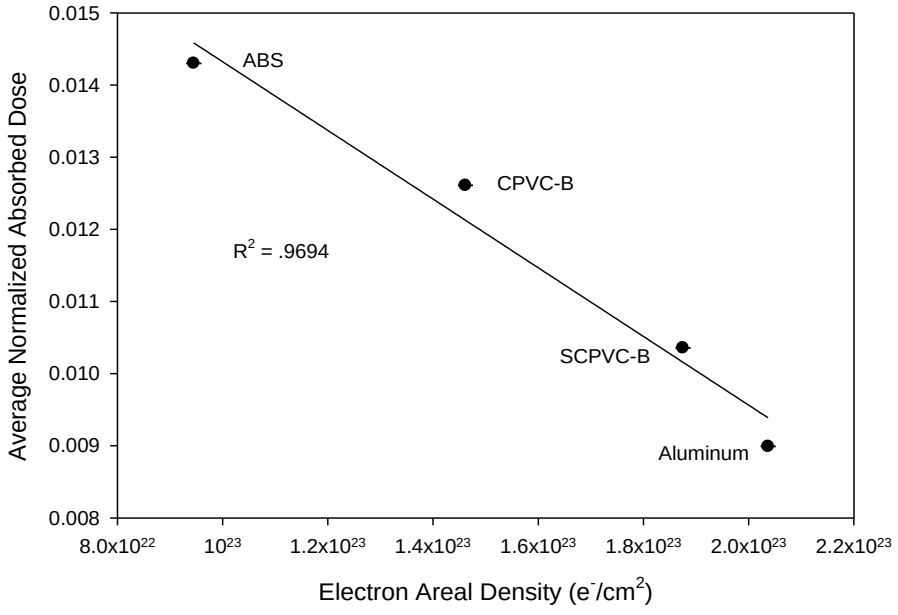

Figure 4.8 – Shows the dose measured by each detector, corrected for air content, normalized by the dose measured by the beam monitor, averaged and plotted as a function of the electron areal density of the detector wall.

The differences in absorbed doses measured by the detectors were proportional to the differences in density of the wall materials from which they were constructed. This demonstrates that the concentration of atoms in a material increases the probability of photon interaction, which reduces the intensity of the beam and also decreases the range of photoelectrons produced in the wall. These effects reduce the number of photoelectrons originating in the innermost portion of the wall that can deposit energy in the gas. It also reduces the number of photoelectrons created in the gas. The overall result is a decreased number of measurable ion pairs being created in the gas of detectors made with increased density of wall material.

4.3.1.2 Half Value Layer (HVL)

The HVL of aluminum is the thickness of aluminum required to attenuate the intensity of an x-ray beam to half of its original value. The HVL should be a constant property of a given x-ray beam and a means to define the quality or penetrating ability of the beam. Each detector was used to measure the HVL of the x-ray beam. The HVL was measured by successively adding layers of aluminum between the source and the detector and measuring the charge collected in the detector for each thickness. The charge measured by the detector was normalized to the charge measured by the beam monitor. The normalized charge was plotted for each detector as a function of attenuator thickness. The data points were then fit with an exponential function to find μ, the linear attenuation coefficient. Based on Equation 2.1, when $\frac{N}{N_0} = \frac{1}{2}$, where x is the thickness of the absorber, it can be shown that:

$$x = HVL = \frac{.693}{\mu}. \tag{4.5}$$

It should be noted that μ is specific to a single photon energy and the given attenuating material. Since the source of x-rays in these experiments produces a spectrum of photon energies,

the μ obtained from a linear fit is not the true value but an average μ. However, the data from all detectors were fit to the same equation, so the determination of each value of μ was consistent. Table 4.2 shows the measured HVL and μ determined from the exponential fit of the attenuation data for each detector. Figure 4.9 shows the exponential fit of the attenuation data measured by the SPVC-B detector.

Table 4.2 – The measured HVL and linear attenuation coefficient measured by each detector. The last two columns show the normalized absorbed dose presented in section 4.3.1.1 for comparison to measured HVL.

Ionization Chamber	μ (mm^{-1})	HVL (mm Al)	Ionization Chamber	Average Normalized Dose
ABS	0.3110	2.23	ABS	0.01430
CPVC-B	0.1822	3.80	CPVC-B	0.01261
Aluminum	0.1812	3.82	SPVC-B	0.01041
SPVC-B	0.1668	4.15	Aluminum	0.00899

The HVL values determined by the three plastic detectors increase with increasing wall density. The HVL values measured by the three plastic detectors also increase with decreasing normalized absorbed dose measurements. The aluminum detector, however, attenuated the beam the most as shown in the absorbed dose measurements but did not measure the greatest HVL. The HVL for the aluminum detector was 3.82 mm, which is comparable to that of the CPVC-B detector at 3.80 mm.

If a monoenergetic x-ray beam were being attenuated, the data in Figure 4.9 would follow a straight line. However, x-rays produced by an x-ray tube form a continuous spectrum of photon energies. Due to the nature of photon interaction with matter, lower energy photons are attenuated preferentially, increasing the average photon energy of the spectrum. [3] This effectively changes the quality or hardness of the beam which in turn means that the attenuation of the beam is no

longer exactly exponential. The slope of the attenuation curve decreases and the subsequent HVLs become greater. [3] This fact is illustrated in Figure 4.9, as the data points do not exactly follow the straight line of the exponential fit.

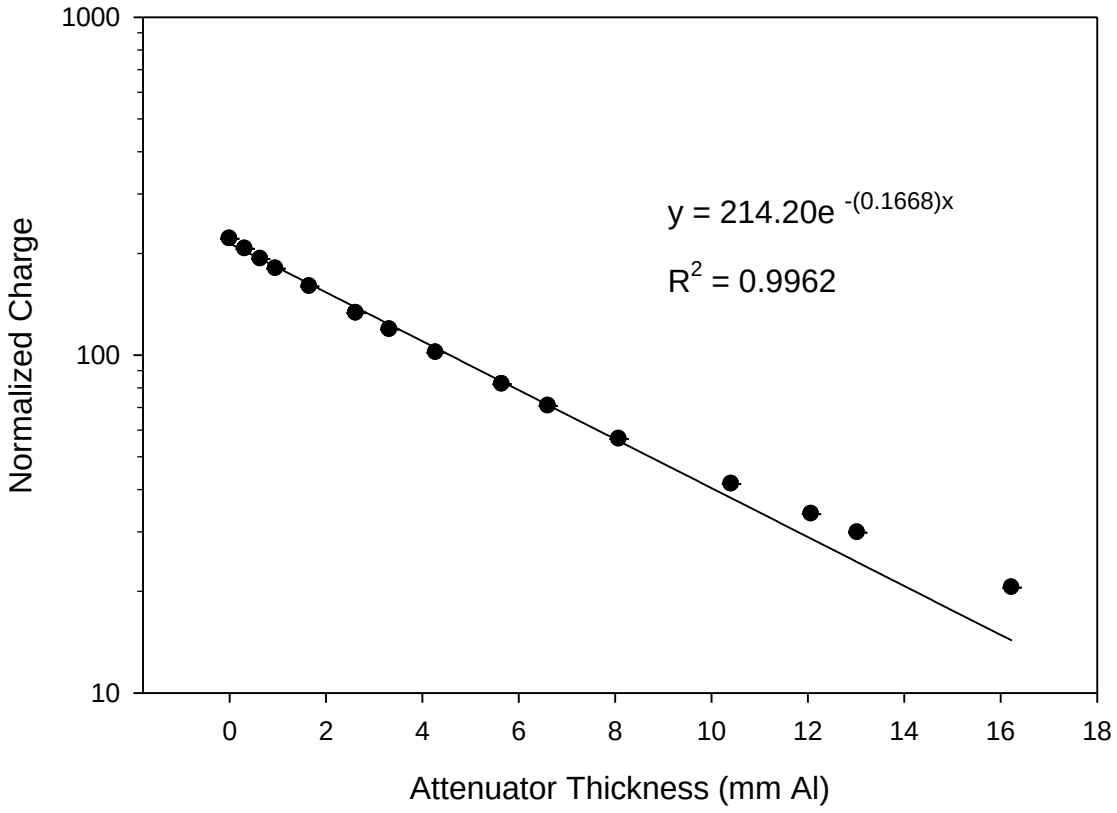

Figure 4.9 - Shows the charge collected by the solid core PVC basic detector (SPVC-B) normalized by the charge collected by the beam monitor, for each thickness of aluminum attenuator.

Table 4.4 shows the HVL and goodness of fit, R^2, values for the HVL measurements made with the four experimental detectors of differing wall composition. Consider that a more filtered beam is closer to a monoenergetic beam since the variation of photon energies in the spectrum has been reduced. An already hardened beam would change less with the addition of attenuators. The less the slope of the attenuation plot changes with the addition of attenuators, the less the change to the photon energy spectrum and the greater the R^2 value would be. So if we

consider the R^2 values for each of the detectors, we should see that the beam is in fact being filtered by our detectors based on the curve of the attenuation graphs. In fact, this is the case and once again the ion chambers are grouped by wall material. The attenuation plot for the aluminum detector is shown in Figure 4.10. In Table 4.3, the aluminum detector is where it is expected to be.

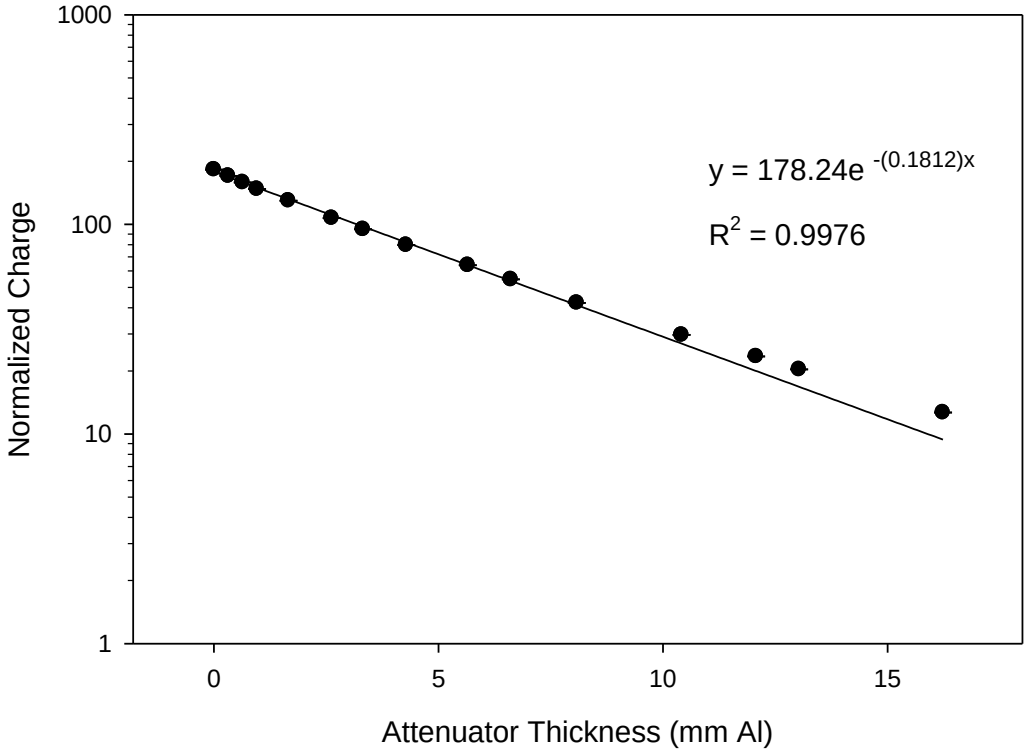

Figure 4.10 - Shows the charge collected by the aluminum detector normalized by the charge collected by the beam monitor, for each thickness of aluminum attenuator.

Table 4.3 – The R^2 values of the exponential fit of the attenuation data for each detector.

Ionization Chamber	HVL (mm Al)	R^2 Value
ABS	2.23	0.9821
CPVC-B	3.80	0.9945
SPVC-B	4.15	0.9962
Aluminum	3.82	0.9976

In conclusion, the R^2 values confirm the hypothesis that the walls of the detectors are filtering the beam to the point that the beam incident on the gas inside each detector is exposed to a different photon energy spectrum. It is clear that the detector walls are thick enough to disturb the photon energy fluence of the beam. It is reasonable to assume that the detector walls would have a different effect on the beam as each aluminum attenuator is added because the photon spectrum incident on the detector will change with each layer of aluminum. The combination of attenuators (the aluminum and the wall of each detector) makes for a complicated situation for which the results may not have a simple explanation. The fact that the aluminum detector is made of the same material as the attenuators may be important in explaining why that detector responds differently as compared to the other detectors. The results also demonstrate the necessity of standardization and conformity in medical and health physics.

The HVL values measured by the four experimental detectors was not compared to that measured with the calibrated PTW-958, because of the considerable size difference of the detectors. The PTW is a small thimble type ion chamber only a few millimeters wide. Based on the lateral field of the x-ray beam displayed in Figure 4.1, it is clear that the photon energy fluence "seen" by the large detectors would be very different from that experienced by the PTW centered in the beam. It should also be noted that the charge measured by each detector was not corrected for temperature and pressure for the HVL determination. The change in mass of air would be insignificant considering we are essentially comparing the shapes of the attenuation

curves and the shape of the curve should remain the same despite small differences in the mass of the air. All of the other attenuation plots are shown in Appendix A.

4.3.1.3 Polarity Effect

In clinical dosimetry there is a polarity effect correction factor that is applied to absorbed dose measurements to correct for changes in readings due to changes when the applied voltage polarity is reversed. It is essentially a measure of the difference in the amount of charge collected when the applied voltage is such that the central electrode is collecting positive ions or negative ions. The calibration certificate provided by the standards laboratory for the PTW-958 stated that the polarity effect was $\leq 1\%$. It is recommended by Khan [3, 6] that the difference should be less than 0.5%. Rather than calculate a correction factor, the percent difference was calculated to compare with the standards laboratory analysis of the PTW-958. The charge measured by each detector for a given polarity was normalized by the charge measured by the beam monitor. Table 4.4 shows the percent difference for the average normalized positive charge collected versus the average normalized negative charge collected.

Table 4.4 – Shows the percent differences in the average normalized charge collected with positive and negative detector bias polarities.

Ionization Chamber	Polarity Effect
ABS	0.0 %
CPVC-B	0.7 %
SPVC-B	0.3 %
Aluminum	4.2 %

The ABS and the solid core PVC detector were under the recommended standard of 0.5% difference in amount of charge collected when applying the opposite polarity. The cellular core detector was under 1% difference and the aluminum detector was well outside of the recommended standard at 4.2%. The cause of this difference is unknown. It was interesting to note that most of the detectors collected more charge when the polarity was set to collect positive

ions. This was unexpected because the gas volume should contain free electrons, and positive and negative ions. The mobility of free electrons is much greater than that of the more massive ions so one would expect to find a greater efficiency when collecting negative charges if there was any difference.

4.3.1.4 Operating Voltage

The applied voltage to all of the detectors was predetermined by preliminary experiments in the developmental stage of the ion chamber design and construction part of this project. All detectors were operated at -600 V, to the cylinder walls, during absorbed dose and HVL evaluations. The operating voltage tests were used to analyze the relative stability of the response of each detector throughout the plateau region of the applied voltages. This was used to determine if small fluctuations in the DC power supply would cause significant differences in detector response. All of the detectors were inefficient at collecting all of the charge produced through the first few hundred volts, but the general trend of responses in the 300 V to 750 V range was less than 1% difference for all but one detector. The normalized charge measured by the SPVC-B detector varied 1.0% between 300 V and 750 V. All plots of applied voltage trials are shown in Appendix B.

4.3.2 Leakage Current Guard Ring

The brass leakage ring of the cellular core PVC basic ion chamber was replaced in the CPVC-R model with a superficial ring that only rested on the interior surface of the detector endcap instead of completely penetrating the endcap as the guard ring in the basic model does. While absorbed dose, HVL, polarity, and operating voltage were measured with each detector, the main purpose of this design was to determine if the simpler guard ring design would be adequate to protect the signal from leakage current or if the complete isolation of the electrode assembly was necessary.

In order to determine if leakage current was significant for either detector, a measurement of the background signal was taken for 15 seconds with the applied voltage set to +600 V. Five such background measurements were averaged and compared with the average charge collected during irradiation for the same amount of time for each detector. The average background measured by the CPVC-R detector was approximately 51 pC which accounted for 0.2% of the average charge collected during irradiation for the same amount of time. The average background measured by the CPVC-B detector accounted for only 0.1% of the average charge measured during irradiation. Although, the detector with the superficial leakage ring did collect more charge on average during background measurement, suggesting that slightly more current was leaked across the protective barrier, the average background charge measured by both detectors was insignificant compared to the average charge collected during irradiation.

The dose measured by each detector was normalized by the dose measured by the beam monitor each time. The normalized absorbed dose of the CPVC-R detector was compared to the normalized absorbed dose of the CPVC-B detector. The CPVC-R detector measured 0.8% more absorbed dose than the CPVC-B detector. This increase concurs with the increase in background measured by the CPVC-R detector, so it is possible that leakage current could be slightly higher in the CPVC-R ion chamber with the simplified guard ring.

The HVL was measured by both detectors following the same procedure described in the previous sections. The CPVC-B detector measured an HVL of 3.80 mm of aluminum, while the CPVC-R detector measured an HVL of 3.82 mm aluminum. For practical purposes, the difference in these to measurements is insignificant.

Both detectors measured less than 1% difference when measuring charge with positive and negative polarity. Only the CPVC-R measured less than the 0.5% difference suggested in the literature. Both detectors were also very stable throughout the range of operating voltages tested.

The normalized charge measured by the CPVC-B detector only varied by 0.2% from 300 V to 750 V and the normalized charge measured by the CPVC-R varied by 0.6% over the same voltage range.

Table 4.5 – Shows the quantities measured by the CPVC-R and the CPVC-B detectors. The polarity effect is the percentage difference in the average normalized charge collected using positive and negative detector bias.

Ionization Chamber	Average Normalized Absorbed Dose	HVL (mm)	Polarity Effect
CPVC-B	0.01261	3.80	0.7%
CPVC-R	0.01271	3.82	0.2%

Table 4.5 shows that there was very little difference in the overall response of the two detectors. For detectors with a volume as great as the ones constructed for this project, it appears that the choice of leakage current guard ring was not a critical factor in the performance of the detectors.

4.3.3 No Leakage Current Guard Ring

The kind of leakage current guard ring was shown to be insignificant to detector response for the cellular core PVC detector constructed. The response of the solid core PVC basic model was compared with a solid core PVC ion chamber with no leakage current guard ring to determine if the electrical resistivity of the PVC was great enough to inhibit leakage current or if a guard ring was necessary to protect the signal quality. In the SPVC-NR detector, only bare PVC separated the central electrode from the wall of the detector. The measured values for the solid core PVC basic model and the SPVC-NR ion chamber are shown in Table 4.6.

Table 4.6 – Shows the relevant quantities measured by the SPVC-B and SPVC-NR detectors.

Ionization Chamber	Average Normalized Absorbed Dose	HVL (mm)	Polarity Effect
SPVC-B	0.01041	4.16	0.3%
SPVC-NR	0.01036	4.17	0.3%

The average background measured by the SPCV-NR was about 17 pC, or less than 0.1% of the average charge measured during irradiation. The average background of the solid core basic model (SPVC-B) was much more stable, only measuring 4 pC. This accounted for less than 0.1% of the average normalized charge measured during irradiation. The basic design, employing a full cylinder brass ring, measured less average normalized charge for the background trials, but what this variation showed was that PVC was very successful in insulating the central electrode from leakage current and that the leakage that did occur was insignificant.

The SPVC-NR ion chamber measured only 0.6% less normalized dose on average than did the basic model. The HVL and polarity effect measured by the two detectors was almost identical. Throughout the 300 V to 750 V range of the operating voltage test, the variation in the amount of normalized charge collected by the SPVC-NR and the SPVC-B detector was about 1.0%. There was virtually no difference in the response of the SPVC-B and SPVC-NR detectors across all of the tests performed, indicating that the lack of a leakage current guard ring did not affect the response of the solid core PVC detector significantly.

4.3.4 Interior Conducting Material

The cellular core PVC was used to test the effects of using a sheet of aluminum foil as the inner conducting surface in the CPVC-Al detector as opposed to the standard graphite spray used in the basic CPVC-B model. The superior conductivity of the aluminum inside the CPVC-Al could effect the charge collecting efficiency of the detector. The results of the absorbed dose, HVL and polarity effect measurements are listed in Table 4.7.

Table 4.7 – Shows the relevant quantities measured by the CPVC-B and CPVC-Al detectors.

Ionization Chamber	Average Normalized Absorbed Dose	HVL (mm)	Polarity Effect
CPVC-B	0.01261	3.80	0.7%
CPVC-Al	0.01175	3.78	0.0%

The average normalized dose measured by the CPVC-Al detector was 6.8% less than that measured by the CPVC-B. This was the greatest discrepancy among any of the basic model variations tested. Rather than showing an improvement in the collecting efficiency, the increased attenuation of the beam by the aluminum foil overshadowed any effect that the increased conductivity of the wall may have had. The results of the tests of detectors made from different wall materials showed that the increased density of the wall material attenuated the beam. The aluminum foil most likely stops most of the electrons liberated in the PVC wall. Although the thickness of the layer of graphite on the other detectors is not known exactly, it is considerably thinner and of lower atomic number than the aluminum foil. In a sense, the addition of aluminum foil inside the detector increased the density of the wall as a whole. An interesting experiment for future work would be to cover the outside of the detector with a layer of aluminum foil and coat the interior with graphite. The idea would be that the greater atomic number of the aluminum foil would increase the production of secondary electrons and the PVC would not be as effective at stopping the secondary electrons as the aluminum foil on the interior. It is hypothesized that the effects of such a test would produce an absorbed dose greater than that measured by the CPVC-Al detector, but still less than that of the CPVC-B detector due to the aluminum still having significant attenuation effects. The absorbed dose of the all three CPVC detectors is plotted in Figure 4.12 to illustrate the relative differences in detector response.

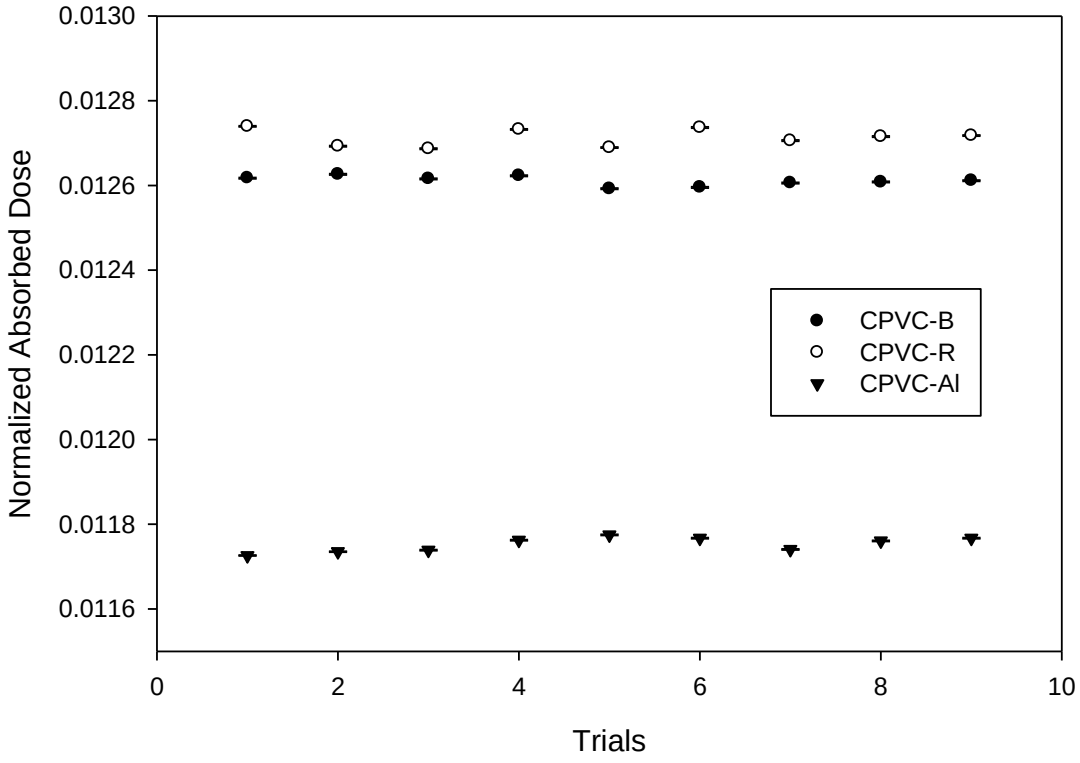

Figure 4.11 – The normalized absorbed doses of the three cellular core ion chambers.

The HVL measured by the CPVC-Al is .02 mm less than that measured by the basic detector. In practical terms, this is insignificant. It should also be noted the difference between the HVL values measured between the CPVC-Al and CPVC-B models is the same difference between the HVL values measured by the CPVC-R and CPVC-B models that consist of exactly the same wall materials. The R^2 values of the attenuation curves of the CPVC-Al and CPVC-B detectors are consistent with the expected results in reference to Section 4.3.2.1 and are listed in Table 4.8. The R^2 value of the CPVC-Al detector is slightly greater than that of CPVC-B demonstrating that the photon energy fluence on the inside the CPVC-Al detector was closer to monoenergetic than that of the basic model.

Table 4.8 – The R^2 values of the exponential fit of the attenuation data for each detector.

Ionization Chamber	R^2 Value
CPVC-B	0.9945
CPVC-Al	0.9947

The polarity effect of the CPVC-Al detector was quite low, less than 0.1%, which is well under the recommended 0.5%. Throughout the 300 V to 750 V range of the operating voltage test, the charge collected by the CPVC-Al ion chamber varied by 0.4%, indicating that slight fluctuations in detector bias will not affect the amount of charge collected significantly.

The effects of the aluminum foil on the interior surface of the wall were apparent in the absorbed dose measurements, but not on the measured HVL values. The aluminum did not seem to effect the ion chamber's consistency or efficiency.

4.3.5 Electrode Surface Area

The electrode of the solid core PVC basic design was replaced with an electrode having much less surface area to determine the effect it would have on collection efficiency. The more slender electrode of the SPVC-SE also effected the geometry of cavity. The downsizing of the electrode significantly increased the interior volume of gas. This change increases the mass of air available for ionization, but also increased the distance that the ion pairs have to travel to be collected. The intention of this variation was to change one design parameter, but in actuality the system became more complex than anticipated. The results of the absorbed dose, HVL value and polarity effect measurements are listed in Table 4.9.

Table 4.9 - Shows the relevant quantities measured by the SPVC-B and SPVC-SE detectors.

Ionization Chamber	Average Normalized Absorbed Dose	HVL (mm)	Polarity Effect
SPVC-B	0.01041	4.15	0.3%
SPVC-SE	0.01055	4.13	0.9%

The SPVC-SE detector measured slightly more absorbed dose than the basic model. Since there was only about 1.3% difference in the measurements, and the background measured by the SPVC-SE detector was insignificant, the source of the discrepancy is unknown. The polarity effect and the variation of charge measured during the operating voltage test were both less than one percent for the SPVC-SE detector. The HVL measured by the SPVC-SE and the basic model were very similar and the 0.02 mm difference was insignificant for practical purposes. Overall, the choice of electrode did not affect the response of the detectors in any significant way.

4.3.6 Chamber Pressure

4.3.6.1 Absorbed Dose to Air

The final variation in detector design was the pressure of the fill gas. For the investigation into the effects of the gas pressure on the response of the detector, a solid core PVC ion chamber capable of being pressurized to several atmospheres was constructed. At the time of data collection, the ambient air pressure was 99600 Pa or approximately one standard atmosphere. The ion chamber was then pressurized to gauge pressures of 1, 2, and 3 atmospheres. The absolute pressures were then approximately 2, 3, and 4 atmospheres. Figure 4.13 shows the charge from the pressurized ion chamber normalized by the charge from the beam monitor for the 10 trials at these pressures.

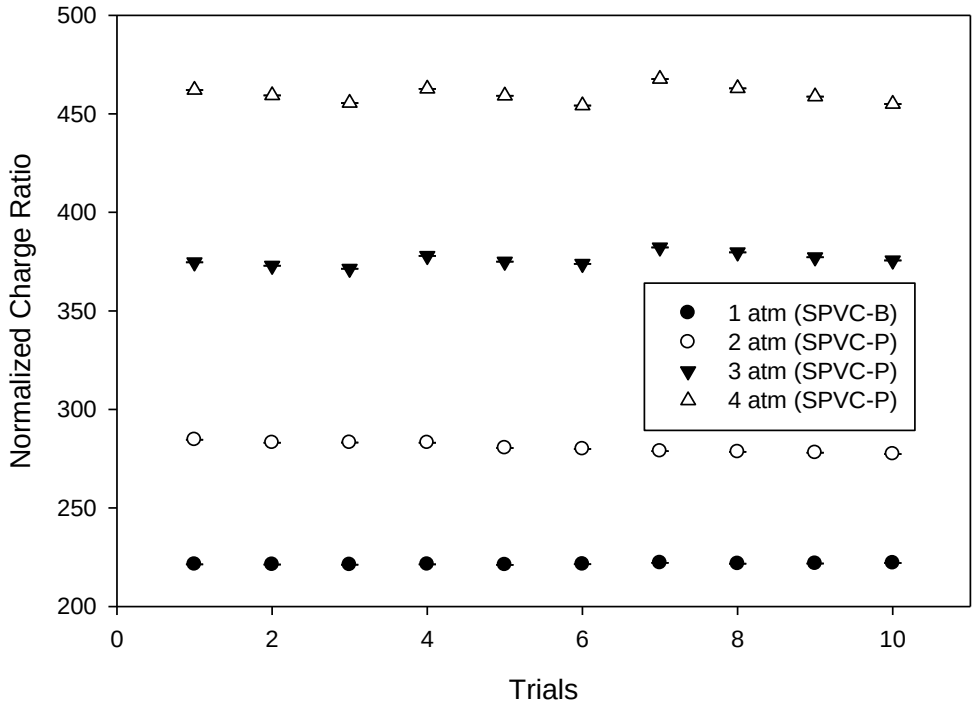

Figure 4.12 – Charge in the SPVC-B ion chamber at ambient pressure and charge in the SPVC-P pressurized ion chamber normalized to charge in the beam monitor for ten trials using pressures of 2, 3, and 4 atmospheres of absolute pressure.

As pressure increased, the amount of charge collected also increased, because the greater density of air increased the probability of photon interaction within the gas, thereby liberating more charge. Figure 4.14 shows the average normalized charge measured at each pressure as a function of pressure. A linear fit of the average normalized charge shown in Figure 4.14 shows that the average charge collected inside the detector increased proportionally with increasing pressure.

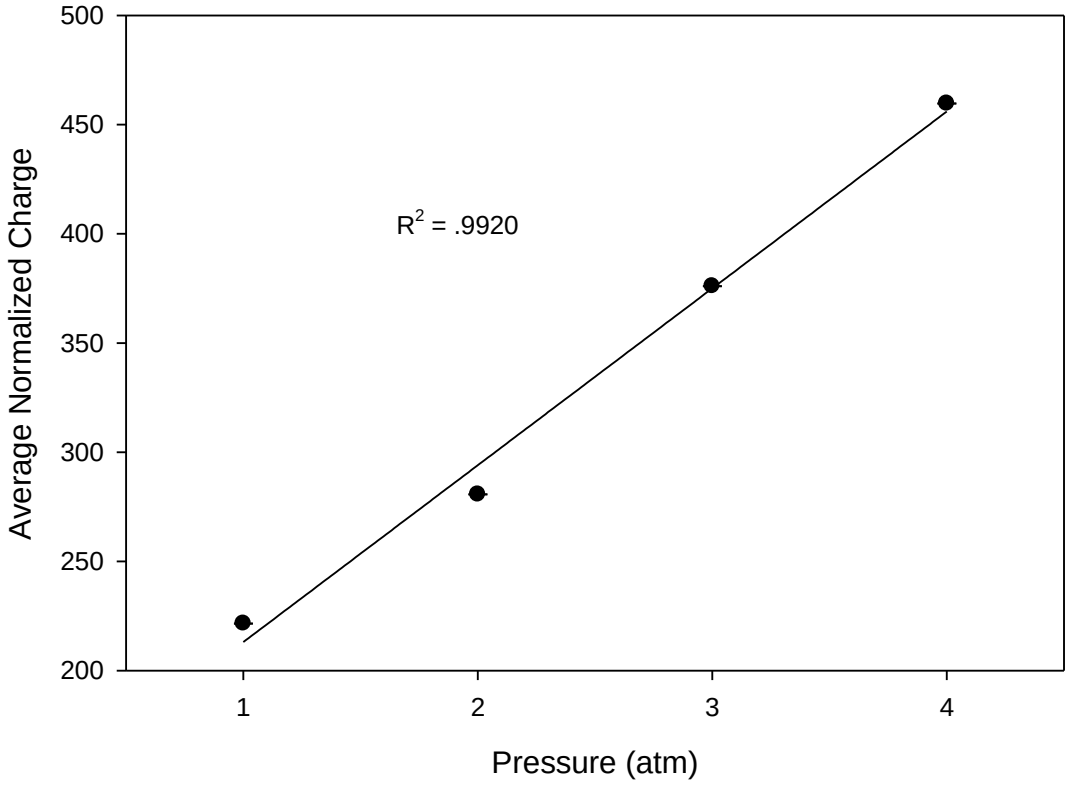

Figure 4.13 – Charge measured by the SPVC-P detector normalized by the beam monitor and averaged over ten trials for each pressure setting.

Figure 4.15 shows absorbed dose measured in the pressurized ion chamber normalized by the absorbed dose measured in the beam monitor for the trials at each of these pressures. Figure 4.16 shows the average normalized absorbed dose as a function of cavity pressure.

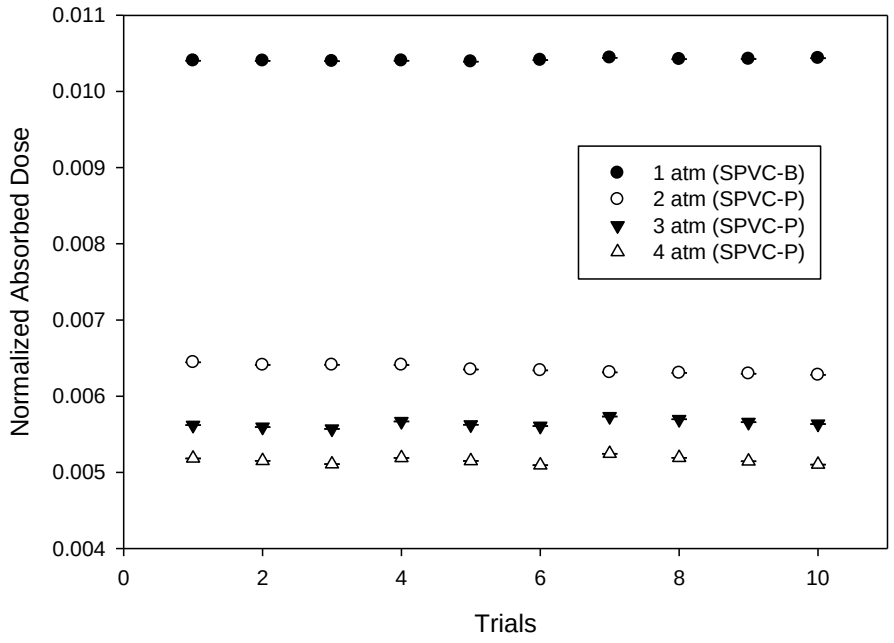

Figure 4.14 – Absorbed dose in the SPVC-B ion chamber at ambient pressure and absorbed dose in the SPVC-P pressurized ion chamber normalized to absorbed dose in the beam monitor for ten trials using pressures of 2, 3, and 4 atmospheres of absolute pressure.

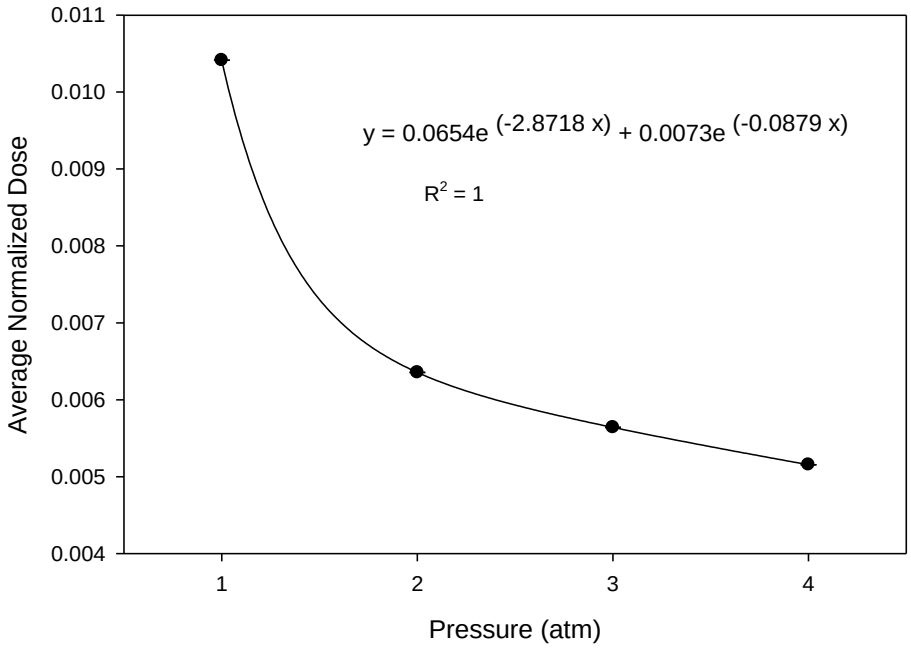

Figure 4.15 – Average normalized absorbed dose measured by the SPVC-P detector normalized by the beam monitor and averaged over ten trials for each pressure setting.

The results of the absorbed dose calculation were unexpected. While the amount of charge increased linearly as a function of pressure, Figure 4.16 shows that the absorbed dose decreased as a function of pressure. This means that although the amount of charge collected in the cavity increased, the mass of air in the cavity increased at a different rate. Therefore, the ratio of charge to mass decreased with increasing pressure.

It is not clear why the amount of charge being collected is not proportional to the number of atoms available for ionization. One hypothesis is that the increased density of atoms in the air cavity reduced the mobility of the ions because the mean free path between collisions of ions and atoms is decreased, which increases the number of opportunities for ion recombination. More ion pairs may have been created than were collected, so the efficiency of the detector was less than 100% when operating at higher pressures. When the concentration of ions is increased, a greater potential is needed to separate the ions before they recombine. When the operating voltage is great enough to collect all of the ions, the detector is said to have reached ion saturation.

A significant observation was made during the operating voltage experiment. The detector response as a function of operating voltage was quite different under high pressure than at lower pressure and also compared to the basic solid core PVC ion chamber, SPVC-B at 1 atm. Table 4.10 shows the amount of variation between the minimum and maximum amount of charge collected throughout the entire range of applied detector biases and specifically the 300 V - 700 V range. The 300 V - 700 V range was used in the discussions in previous sections of the ion chamber variations because this range is believed to be within the plateau region of the applied voltages.

Table 4.10 – The average normalized charge collected at 600 V and the variation in charge collected throughout the ranges of applied detector bias.

Ionization Chamber Absolute Pressure	Average Normalized Charge Collected	Operating Voltage Variation (100 V - 750 V)	Operating Voltage Variation (300 V - 750 V)
1 atm (SPVC-B)	221.56	2.0%	1.0%
2 atm	280.23	3.3%	3.2%
4 atm	459.71	19.0%	4.5%

There was about 19% difference in the minimum and maximum normalized charge collected by the SPVC-P detector pressurized to 4 atm through the entire range of applied voltages. The variation between minimum and maximum response of the SPVC-B and the SPVC-P pressurized to 2 atm was about 2% - 3.5% through the same range of applied voltages. For the higher voltage range over which the other detector variations were examined in previous sections, the variation was much smaller but significant nonetheless. A difference of 3.2% and 4.5% in the normalized charge collected between 300 V – 700 V indicates that the stable ion collecting plateau voltage range may come at a higher voltage for the SPVC-P ion chamber pressurized above ambient pressure. Figure 4.17 shows the operating voltage trials for the SPVC-B ion chamber at ambient pressure (1 atm) and the SPVC-P ion chamber pressurized to two and four atm.

The normalized response became more stable at much lower voltage for the other detectors. The increased inconsistency of detector response of the pressurized detector at higher pressures, shown in Figure 4.13, suggests a possibility that not all of the charge was being collected. These observation lead to the second experiment involving operating voltage.

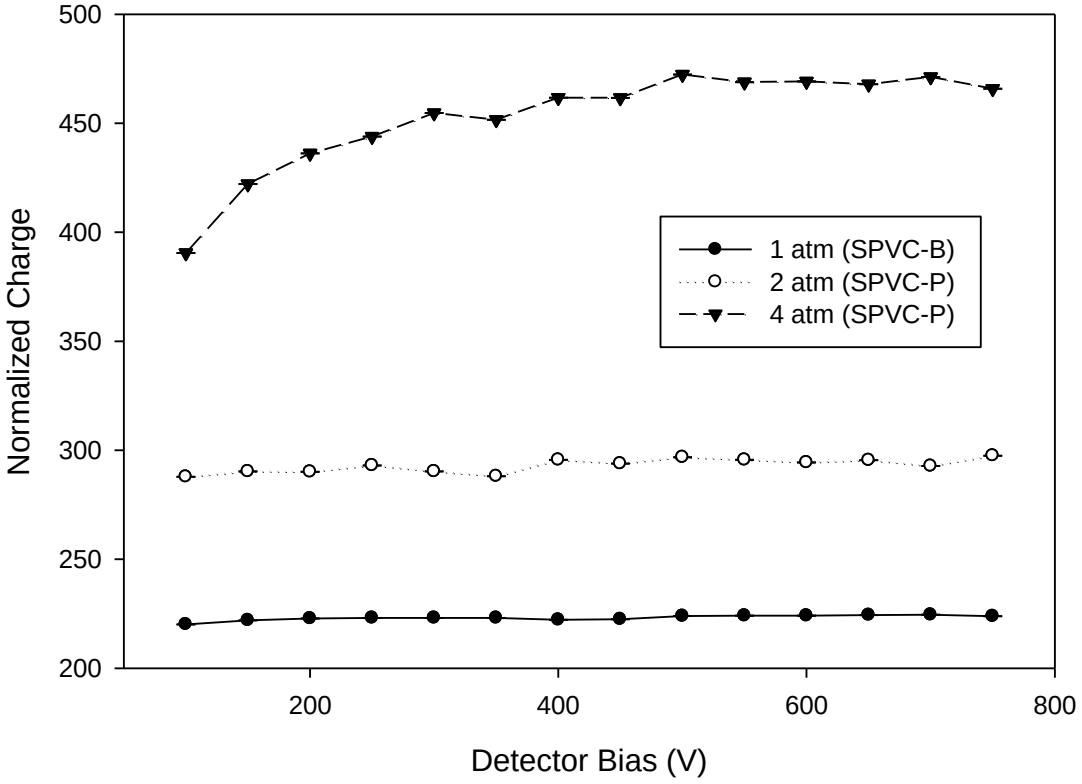

Figure 4.16 – The normalized charge measured throughout the range of operating voltages for the basic SPVC-B detector operated at ambient pressure and the SPVC-P detector operated at 2 atm and 4 atm.

The normalized absorbed dose was measured using an applied voltage of 800 V and compared to the normalized dose of the 600 V trials, shown in Figure 4.19. The absorbed dose measured with the SPVC-P detector increased slightly compared to the response at 600 V. The average doses measured at 600 V and 800 V differed by 3.2%. This evidence supports the hypothesis that the detector was not completely saturated, when operated at higher pressures due to insufficient detector bias which would explain why the absorbed dose measured decreased with increased pressure.

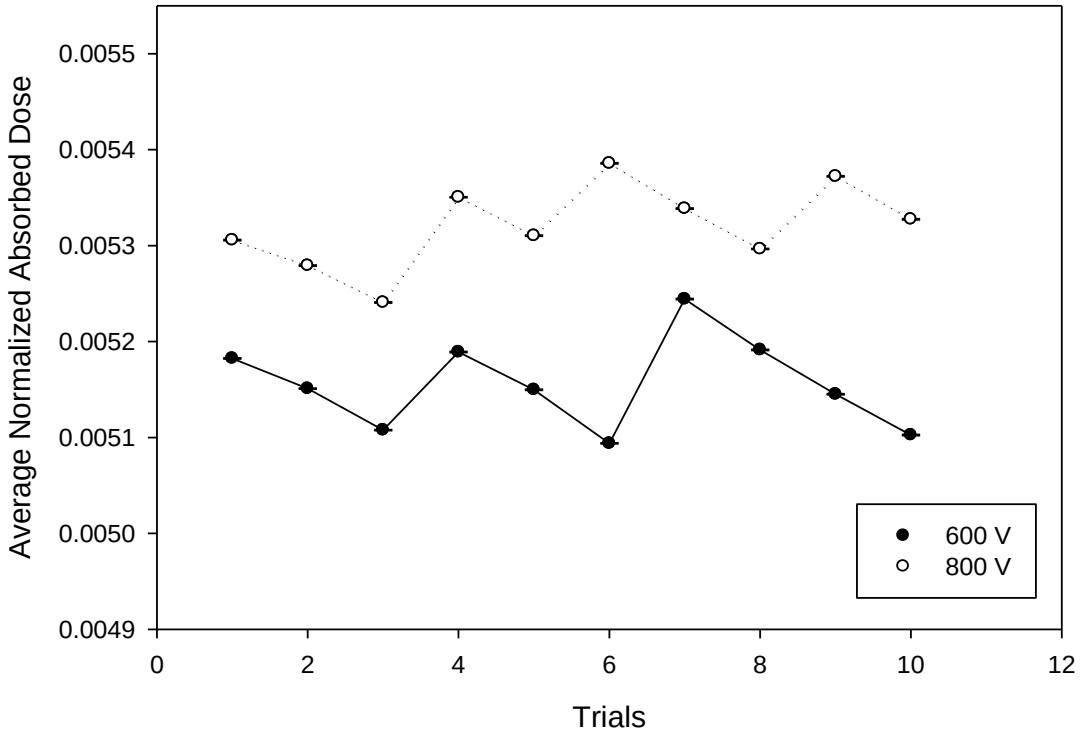

Figure 4.17 – The average normalized absorbed dose measured by the SPVC-P detector while operated at 600 V and 800 V.

4.3.6.2 Half Value Layer

The same procedure used to measure attenuation curves and determine HVL values for all of the other detectors was performed with the pressurized detector. The measured linear attenuation coefficient, HVL, average normalized charge, and average normalized absorbed dose are listed in Table 4.11. The linear attenuation coefficient increased with the increased pressure of gas inside the chamber. The HVL calculated for each pressure decreased linearly as pressure increased as shown in Figure 4.20.

Table 4.11 – Shows the linear attenuation coefficient μ, HVL, average normalized charge and average normalized absorbed dose measured by the SPVC-B and SPVC-P detector pressurized to 2, 3, and 4 atm.

Pressure (atm)	μ (mm^{-1})	HVL (mm Al)	R^2 Value of Exponential Fit	Average Normalized Charge	Average Normalized Absorbed Dose
1 (SPVC-B)	0.1668	4.15	.9962	221.56	0.01041
2	0.1700	4.08	.9960	280.71	0.00636
3	0.1743	3.98	.9953	376.04	0.00564
4	0.1783	3.89	.9952	459.71	0.00515

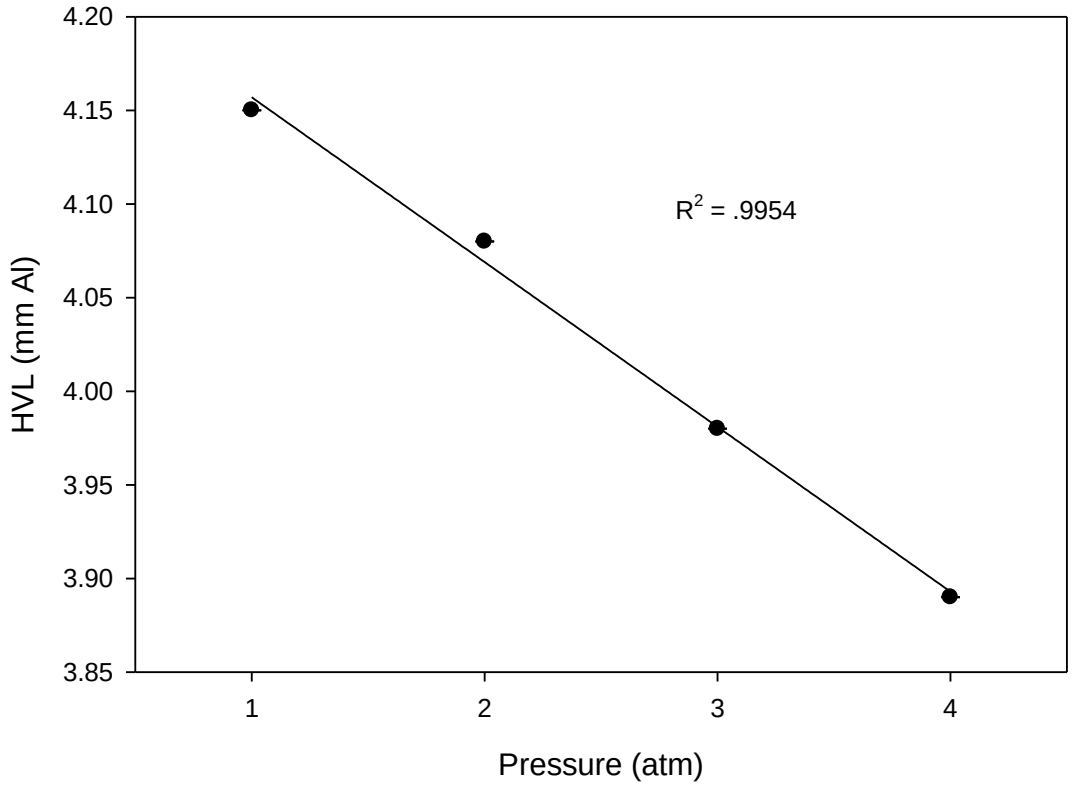

Figure 4.18 – Shows the HVL measured by the SPVC-B ion chamber at 1 atm and the SPVC-P ion chamber pressurized to 2, 3, and 4 atm.

A combination of many variables such as two separate attenuating factors, the low energy photon spectrum being analyzed, the very thick walls of the detectors, and the inefficiency of the

pressurized detectors in collecting all of the charge, suggests that there is no simple explanation for these results. It is remarkable, however, how well a linear function fits the data points of HVL as a function of detector pressure in Figure 4.20, which suggest that maybe there is a single dominating factor producing this trend. Figure 4.21 shows the attenuation curves measured by the SPVC-P detector for the pressures tested. The R^2 values of the exponential fit of the attenuation data are also interesting. As discussed in Section 4.3.1.2, a more attenuated beam would be expected to produce a higher R^2 value of the exponential fit. Table 4.11 shows that the HVL and R^2 values agree in principle but the mechanism that supports their correlation with the air pressure in the cavity remains undetermined.

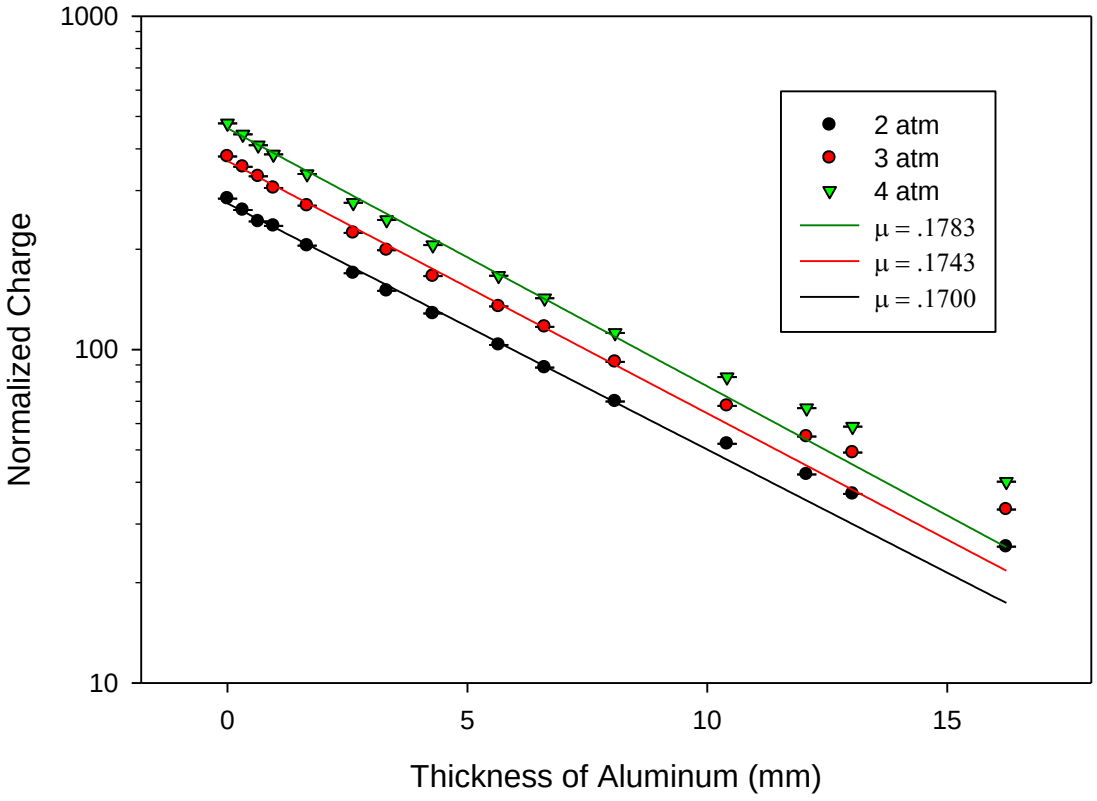

Figure 4.19 – The attenuation curves fit with an exponential function to obtain the linear attenuation coefficient μ, for all three pressure settings.

4.3.6.3 Pressure Conclusion

Although the results from all of the measurements obtained by the pressurized detectors leave some questions unanswered, they do demonstrate some of the core principles of ionization chamber dosimetry. The normalized charge measurements show directly how increasing the density of a substance increases the probability of photon interaction. The decrease in dose measured with increasing air pressure demonstrate the importance of complete ion collection efficiency. Although the HVL values do decrease with pressure, it is important to realize that the values, 4.08, 3.98, and 3.89 mm Al, respectively, are only about .1 mm apart and that this difference is insignificant for practical purposes. The reason for the decrease was not determined.

CHAPTER V

CONCLUSION

The main goal of this project was to construct a set of instruments that students could use in an introductory dosimetry class to give them an experimental basis to learn the theoretical principles taught in lecture and the literature. Nine ionization chambers were designed, fabricated, and characterized by measuring absorbed dose, HVL, operating voltage, and polarity effect. The results of the experiments highlighted some other important concepts of dosimetry, such as, attenuation, ion recombination, and leakage current. All detectors were built in-lab, at low cost from readily available plumbing supplies. The ion chambers were shown to be robust, consistent, and capable of demonstrating some of the fundamental principles involved in radiation measurement. Specific conclusions from the various detectors are summarized below.

5.1 Effect of Wall Material:

The attenuation of the x-ray beam was affected by the different wall materials of the detectors as reflected in the differences in measured absorbed dose. The average normalized dose decreased linearly with increasing areal density and electron areal density. The attenuation of the incident photons and the secondary electrons by the wall material of the detector directly affects the fluence of electrons that travel through the gas and deposit their energy through collisions with atoms in the air in the cavity. So the amount of charge measured and the absorbed dose calculated using each detector is dependent on these photon and electron interactions. By plotting the responses of all of the detectors as a function of detector wall composition, these experiments showed that the probability of these two interactions is highly dependent on the areal density of the material and that measuring the same x-ray beam with two different detectors can produce significantly different results and corrections to measurements should be made accordingly.

The HVL values measured with the four detectors of differing wall material introduce the complexity of radiation interaction with matter. The HVL values measured by the three plastic detectors increase with increasing wall areal density. The effect of the wall material on absorbed dose and HVL when considered together is highly complex. This can especially be seen when comparing the result of the aluminum detector to the results of the plastic detectors. Although the wall of the aluminum detector attenuated the beam the most in terms of absorbed dose, it did not have the greatest measured HVL. The manner in which the attenuation of the x-ray beam, by the wall of the detectors and by the aluminum attenuators, affects the HVL measured by each detector could not be determined with these experiments.

The operating voltage and polarity measurements made by all of the detectors in this thesis project were mainly used to show that the detectors worked properly and consistently. The goal was not to show or explain any significant differences in the measurements. Of all of the

measurements taken with opposite polarity, the aluminum detector showed the greatest percent difference at 4.2% between positive and negative polarity.

5.2 Effect Leakage Current Guard Ring:

The significance of the kind of leakage current guard ring was the subject of the next experiments. The cellular core PVC ion chamber, CPVC-R, used a superficial guard ring on the interior surface of the detector. The amount of background charge measured indicated that the leakage current was very small. The difference in the absorbed dose measured by the CPVC-R compared to the CPVC-B model was insignificant. The differences in HVL values measured by the CPVC-R with respect to the basic model was also insignificant. The CPVC-R detector operated satisfactorily in the operating voltage and opposite polarity tests. The overall result of the tests was that the leakage current guard ring was not a critical component of detectors of this particular design.

5.3 Effect of No Leakage Current Guard Ring:

The SPVC-NR ion chamber measured only 0.6% less normalized dose on average than did the basic SPVC-B model. The background charge measured with no irradiation was insignificant to the total charge collected during irradiation, indicating that leakage current was also not significant. The HVL and polarity effect measured by the two detectors was almost identical and the operating voltage test of the SPVC-NR showed that it operated properly. There was virtually no difference in the response of the SPVC-B and SPVC-NR detectors across all of the tests performed, indicating that the lack of a leakage current guard ring did not affect the response of the detector significantly.

The variations or complete absence of a leakage current guard ring did not have a significant effect on the measurements made with PVC detectors. It should be noted that since the interior space of the ion chambers was so large that there was a significant amount of insulating

material separating the collecting electrode from the electrified wall. If the ion chambers were of the much smaller size, as is used in clinical x-ray beam dosimetry, the leakage current guard ring would likely play a much more crucial role and leakage current would probably be more significant.

5.4 Effect of Interior Conducting Material:

The purpose of the design of the aluminum foil lined ion chamber was to determine if charge could be collected more efficiently by increasing the conductivity of the interior wall. What the results actually showed was that the response of the detector was dominated by the attenuation of the x-ray beam by the aluminum foil. The CPVC-Al detector measured an absorbed dose that was significantly less than that measured by the basic CPVC-B model. Any effect that the aluminum foil had on efficiency was overshadowed. The HVL measured by the CPVC-Al was .02 mm less than that measured by the CPVC-B model. This was a very slight change considering that the absorbed dose measured by the CPVC-Al was 6.8% less than that of the basic model. Of the other plastic detectors considered in the differing wall materials section, the significant difference in absorbed dose was accompanied by a significant difference in measured HVL. The operating voltage and opposite polarity measurements showed that the detector operated satisfactorily.

5.5 Effect of Electrode with Reduced Surface Area:

The SPVC-SE ion chamber was constructed to investigate the effect of reducing the surface area of the collecting electrode on ion collection efficiency, but the reduced size of the electrode increased the volume of air inside the chamber and also increased the average distance that ions would have to travel to be collected. The SPVC-SE ion chamber did measure slightly more dose than the basic solid core PVC model, but whether this could conclusively be attributed to the difference in surface area of the electrode was not determined. It was incorrectly

hypothesized that the reduced surface area of the SPVC-SE electrode and the greater average distance of ion travel would actually reduce the measured absorbed dose to the air of the detector. There was only about 1.3% difference in the absorbed dose measurements of the SPVC-SE and SPVC-B detectors, and the background measured by the SPVC-SE detector was insignificant. The difference in HVL measured by the SPVC-SE ion chamber and the basic model was insignificant while the operating voltage and opposite polarity tests showed the detectors to be working properly.

5.6 Effect of Chamber Pressure:

The pressurized detector produced very significant results that highlight the important concept of ion recombination. While, the normalized charge measurements show directly how increasing the density of a substance increases the probability of photon interaction, the decrease in absorbed dose measured with increasing air pressure demonstrates the importance of complete ion saturation. The charge and absorbed dose measurements suggested that all of the charge that was being created by the ionizing radiation was not collected because the amount of charge increased with pressure but the absorbed dose decreased with pressure. One would expect the number of ionizations to be proportional to the number of targets. Since the experimental measurements did not produce this result it is assumed that not all of the charge that was created was collected by the ion chamber.

The pressurized ion chamber experiments were the only area where the operating voltage tests provided significant information. The operating voltage experiments showed incomplete ion collection was significant at much greater applied voltages for the high pressure setting than with all of the other ambient pressure detectors tested. The average absorbed dose was about 3.6% greater when measured through ten trials when the detector was operated at 800 V than at 600 V.

This suggests that a possible cause of the increased ion recombination during the dose measurements was an insufficient applied operating voltage for that pressure setting.

The plots of charge and absorbed dose versus air pressure appear to show that the measurements taken at higher pressures were more inconsistent. I believe this to be due to inconsistency in the amount of air in the chamber. At higher air pressure the chamber leaked very slowly, so a few irradiations were measured and then the air pressure was adjusted. This process continued throughout the measurements of three and four atmospheres of air pressure. At low air pressure the air did not leak significantly.

The HVL values measured by the detector decreased about 2.5% for each atmosphere of pressure added. For each pressure setting the beam was being attenuated by two materials, the aluminum attenuators and the air inside the cavity, and since it is believed that only some of the total charge produced in the cavity was being collected, the experimental parameters were too complex to warrant a simple relation to the measured trends and the air pressure inside the chamber. In this experiment the greater HVL values did correspond with the greater R^2 values as expected, but why the greater HVL corresponded with the lower pressures was undetermined. Although the HVL values do decrease with pressure, it is important to realize that the values, 4.08, 3.98, and 3.89 mm Al, respectively, are only about .1 mm apart and that this difference is insignificant for practical purposes.

5.7 Summary of Conclusions:

Of all of the variables studied, the dependence of wall composition and thickness on detector response was the most significant, followed by the pressure of the gas in the ion chamber. The design or presence of a leakage current guard ring for this ion chamber size and design did not have much of an effect on detector response. The interior conductivity of the interior wall was dominated by the attenuation of the x-ray beam by the aluminum foil, so the effects of increased

conductivity were not determined. The PVC ion chamber with the slender solid electrode did measure slightly more absorbed dose than the basic model but the difference in HVL values was insignificant. Although the increased air pressure in the PVC increased the charge collected in the detector, incomplete ion collection resulted in the measured absorbed dose being reduced.

5.8 Future Work:

The addition of a few new detectors would improve this work and possibly help clarify some of the results. In the experiments carried out investigating the different detector wall materials, I was comparing wall areal density, which is two things. The experiment would be more instructive if the variables of wall density and thickness could be isolated. Some detectors could be constructed of the same wall material, but of various thicknesses. Likewise, several detectors of the same wall thickness could be constructed from different wall materials. The experiment carried out for this project was approached the way that it was because one constraint of this project was to construct the detectors from low cost readily available materials. Custom designed detectors would have to be specially made and cost more, however, the results would be more definitive.

Another kind of detector I would be interested to make would be a PVC detector with aluminum foil on the outside. It would be interesting to compare the difference of response to that of the CPVC-Al detector constructed with aluminum foil on the inside. I believe that the location of the aluminum foil would change the attenuation properties of the detector wall.

There are a few things that I would do differently if I were to carry out this project again. In the early design process, the decision was made to make all of the interior volumes of the detectors as similar as possible. I would instead, construct all of the detectors to be the same overall length and let the interior volume vary. The absorbed dose calculation takes into consideration the mass of the air inside the chamber, so the interior volume is not as critical. As

was displayed in the plot of the lateral field size inside the El Vacatron x-ray machine, Figure 4.1, the intensity of the beam falls off rapidly towards the outside edges. Ion chambers of different lengths are exposed to a different photon fluence, so it is important that all of the detectors be the same length for an appropriate comparison of the responses.

In the analysis of the individual detectors, I measured the operating voltages as a secondary consideration of this project. The original idea was only to observe that the detector functioned properly and that small variations in the power supply would not significantly affect my measurements. In the literature, there is a mathematical way to describe the ion collection efficiency. For continued analysis, the operating voltage data that was recorded for this project could be used to perform a more rigorous mathematical efficiency analysis of the detector responses.

REFERENCES

[1] H. Johns and J. Cunningham, *The physics of radiology* (Charles C. Thomas, Springfield, Ill., U.S.A., 1983).

[2] K. Knoll, *Radiation detection and measurement* (Wiley, NY., U.S.A., 1979).

[3] F. Khan, *The physics of radiation therapy* (Lippincott Williams & Wilkins, Phiadelphia, PA., U.S.A., 2003).

[4] N. Tsoulfanidis, *Measurement and detection of radiation* (Taylor & Francis, Washington, DC, 1995).

[5] NIST. Stopping-Power and Range Tables for Electrons. <http://www.nist.gov/pml/data/star/index.cfm>.

[6] IAEA. *Absorbed dose determination in external beam radiotherapy* (Vienna, 2000).

[7] K. Kase, *Concepts of radiation dosimetry* (Pergamon, Elmsford, NY., U.S.A., 1978).

[8] H. Rossi, Tissue-Equivalent Ionization Chambers. *Nucleonics* 14 (1956): 32-37.

APPENDICES

APPENDIX A – HALF VALUE LAYER (HVL)

Appendix A shows the attenuation data that was measured by each of the ion chambers and was used to determine the HVL. It includes all of the plots that were not included in the results section of this thesis.

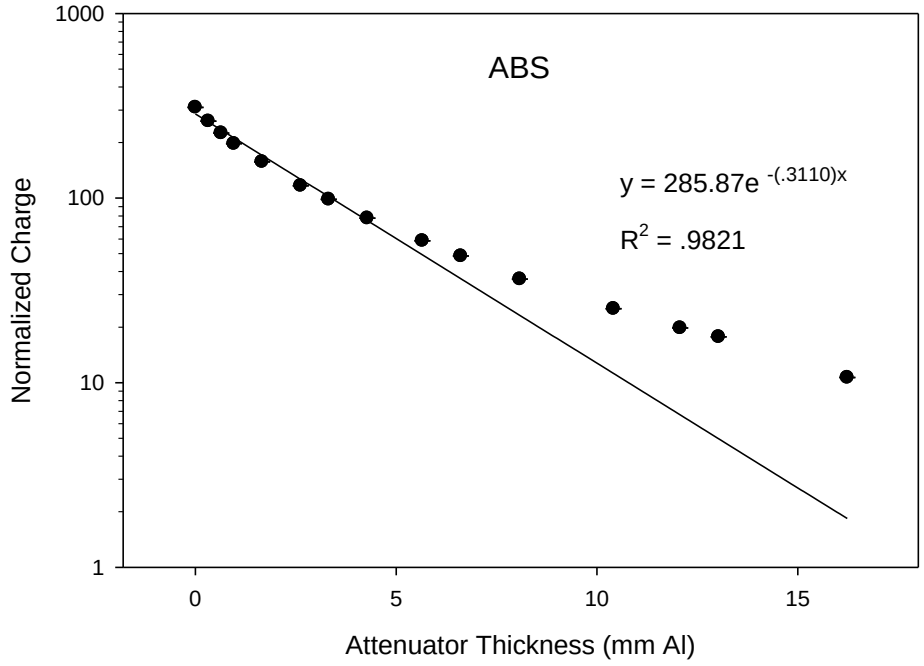

Figure A.1 - Shows the charge collected by the ABS detector normalized by the charge collected by the beam monitor, for each thickness of aluminum attenuator.

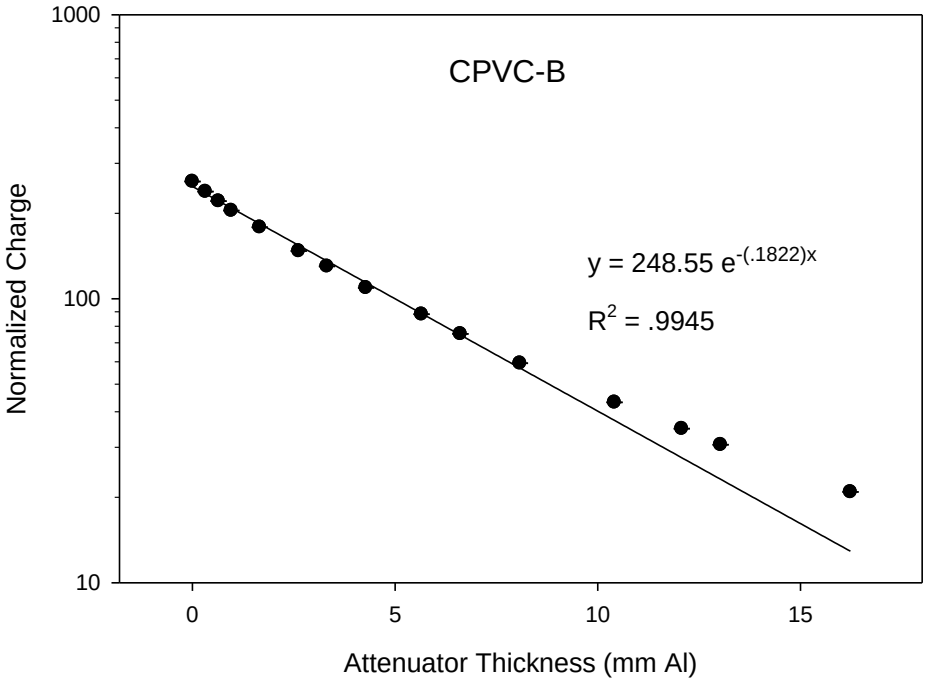

Figure A.2 - Shows the charge collected by the cellular core PVC basic detector (CPVC-B) normalized by the charge collected by the beam monitor, for each thickness of aluminum attenuator.

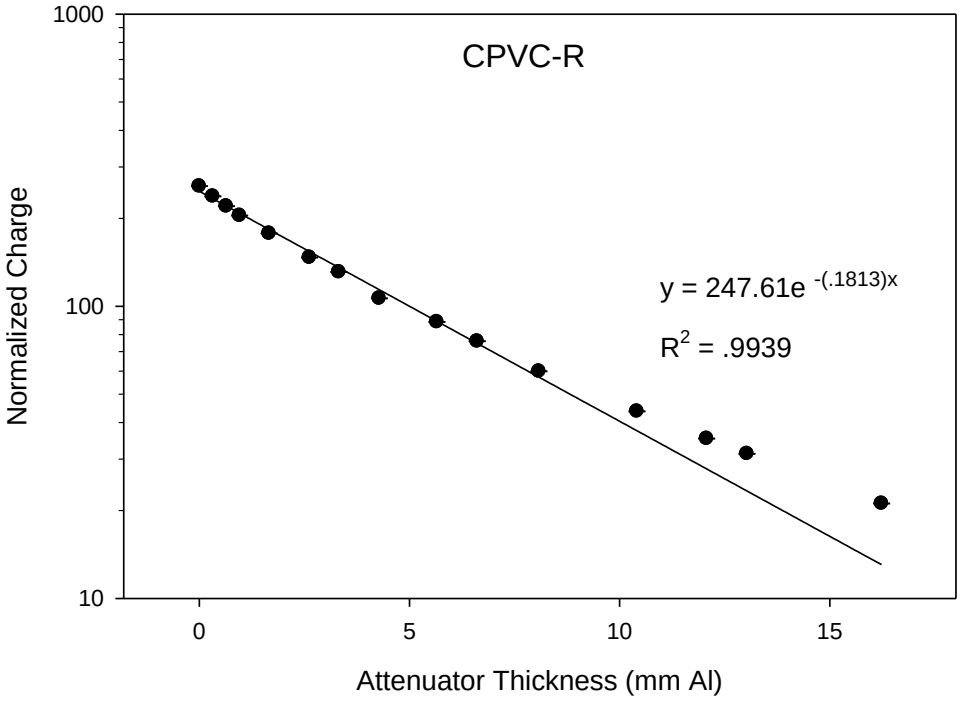

Figure A.3 - Shows the charge collected by the cellular core PVC detector (CPVC-R) normalized by the charge collected by the beam monitor, for each thickness of aluminum attenuator.

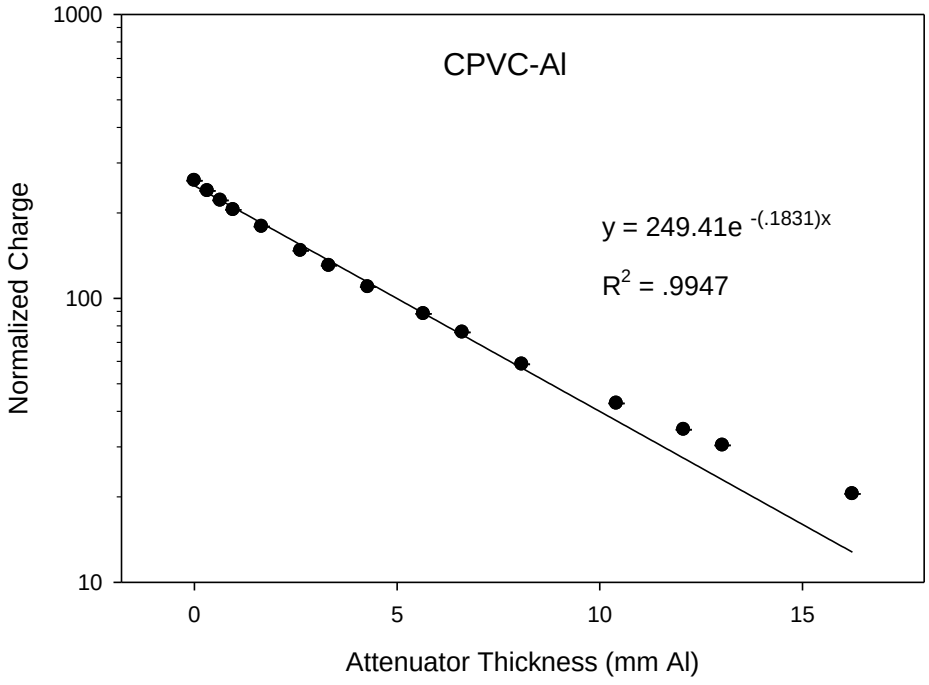

Figure A.4 - Shows the charge collected by the cellular core PVC detector (CPVC-Al) normalized by the charge collected by the beam monitor, for each thickness of aluminum attenuator.

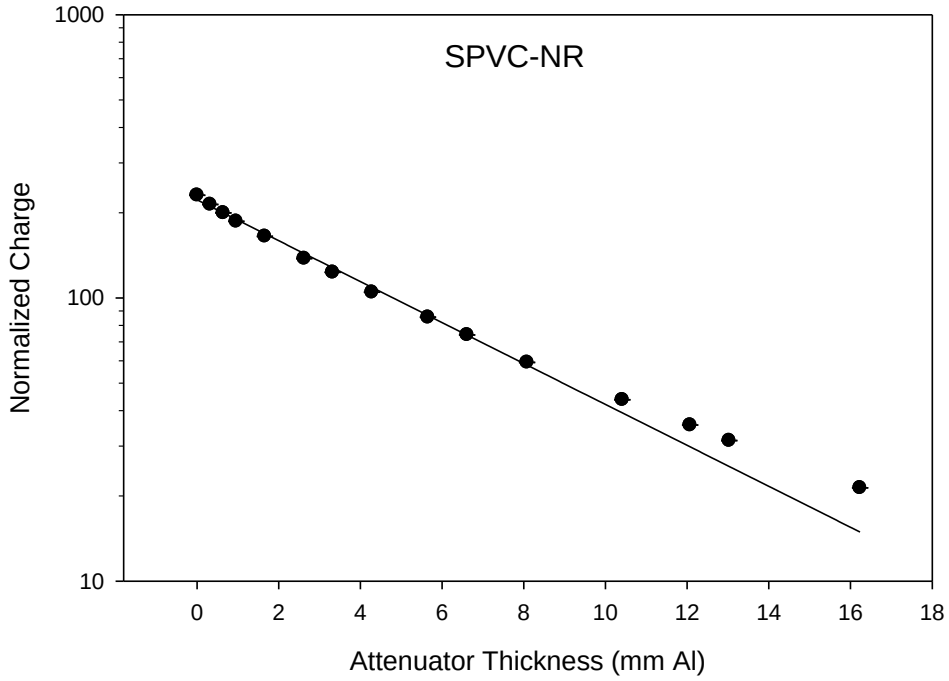

Figure A.5 - Shows the charge collected by the cellular core PVC basic detector (SPVC-NR) normalized by the charge collected by the beam monitor, for each thickness of aluminum attenuator.

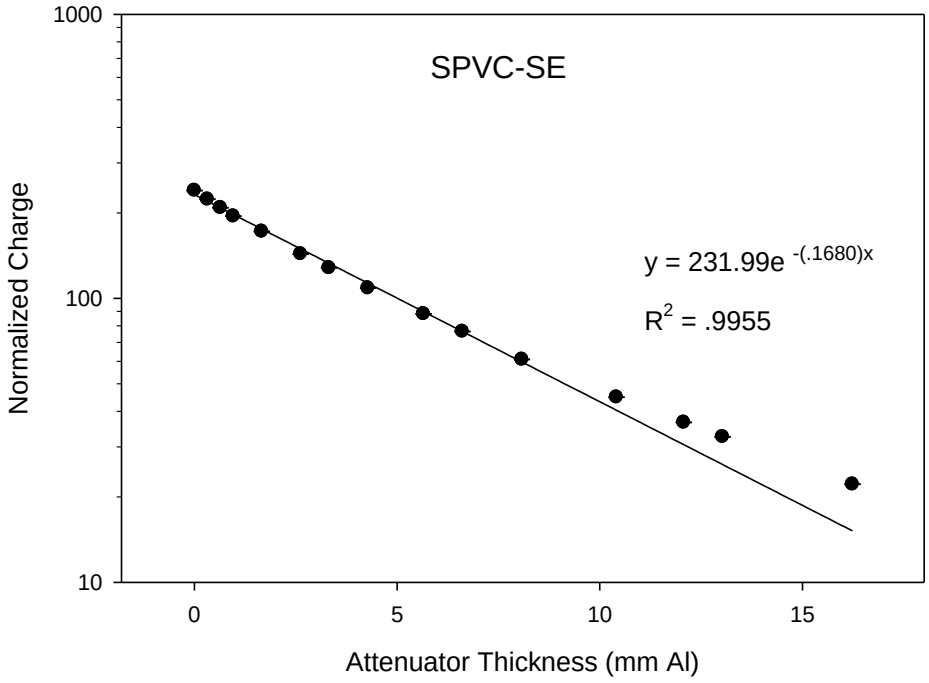

Figure A.6 - Shows the charge collected by the solid core PVC detector (SPVC-SE) normalized by the charge collected by the beam monitor, for each thickness of aluminum attenuator.

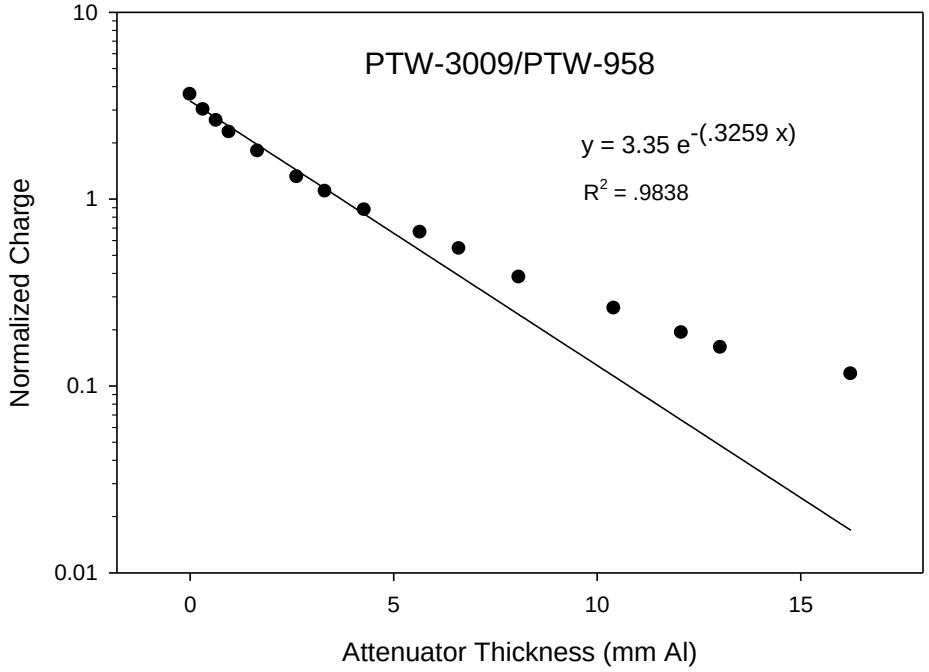

Figure A.7 – Shows the charge measured by a calibrated Farmer type PTW-3009 normalized by the beam monitor PTW-958.

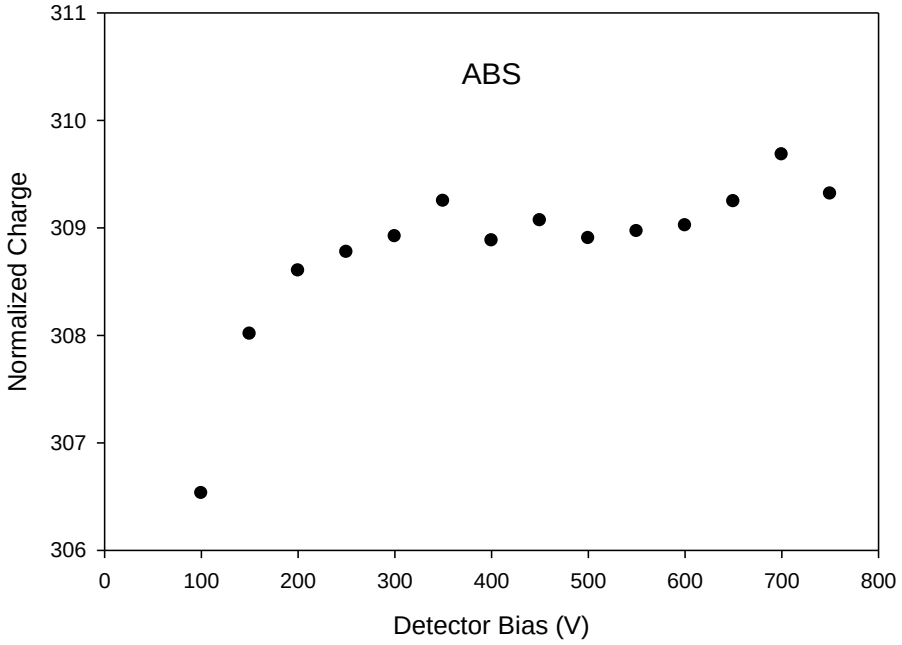

Figure B.1 - Operating voltage trials for the ABS detector.

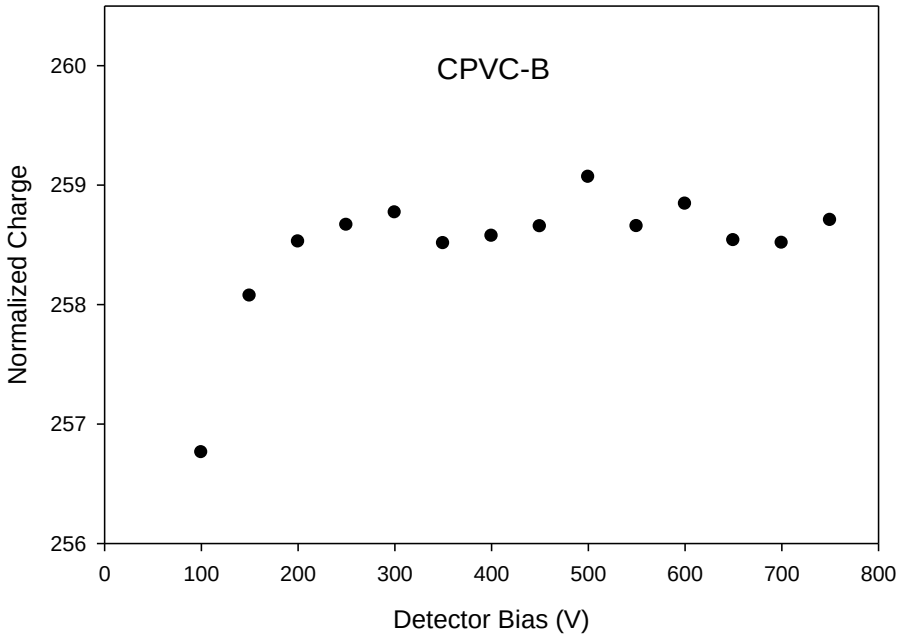

Figure B.2 - Operating voltage trials for the CPVC-B detector.

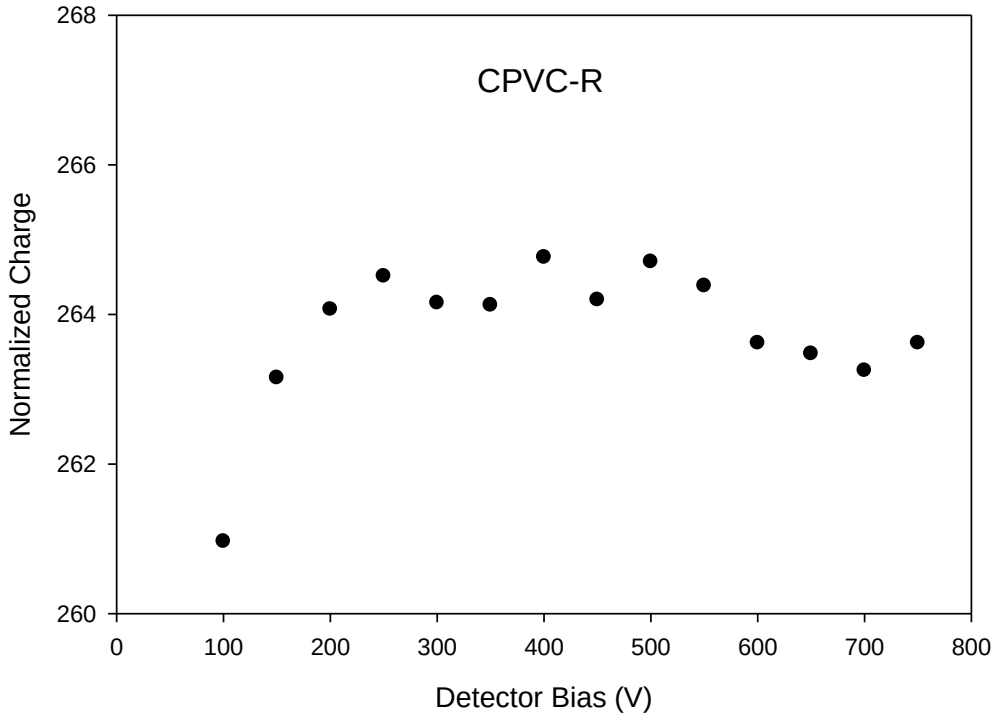

Figure B.3 - Operating voltage trials for the CPVC-R detector.

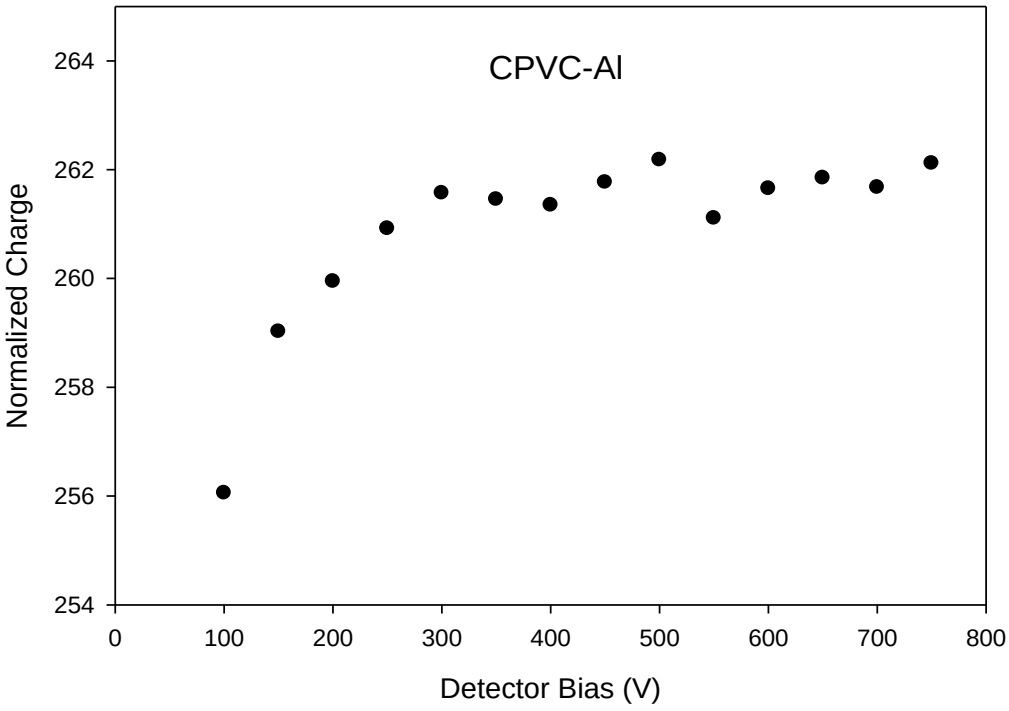

Figure B.4 - Operating voltage trials for the CPVC-Al detector.

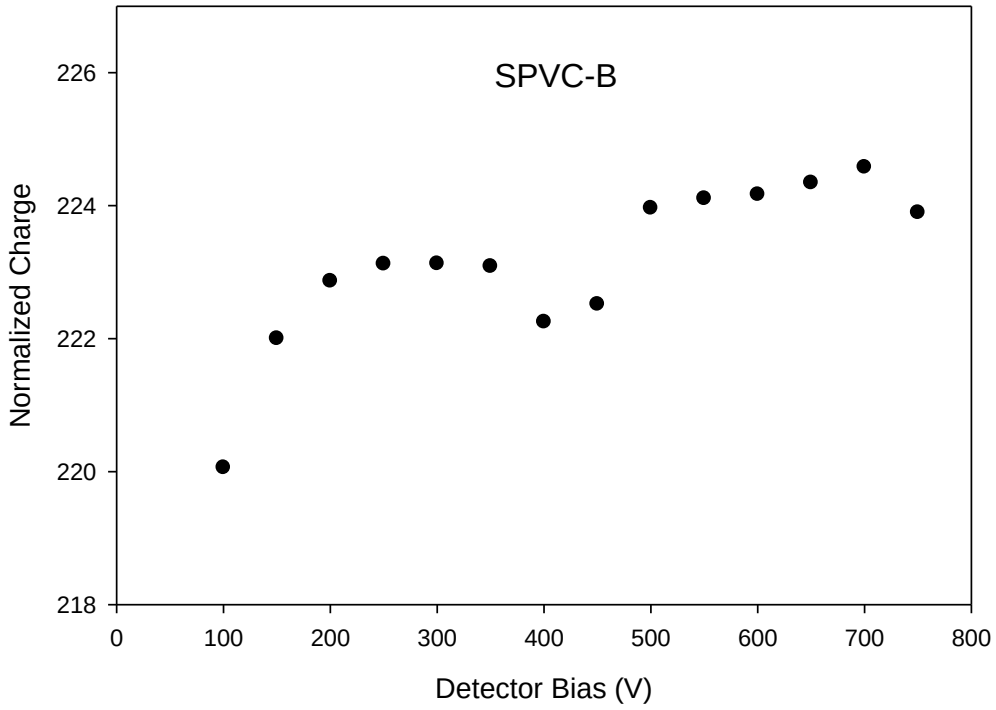

Figure B.5 - Operating voltage trials for the SPVC-B detector.

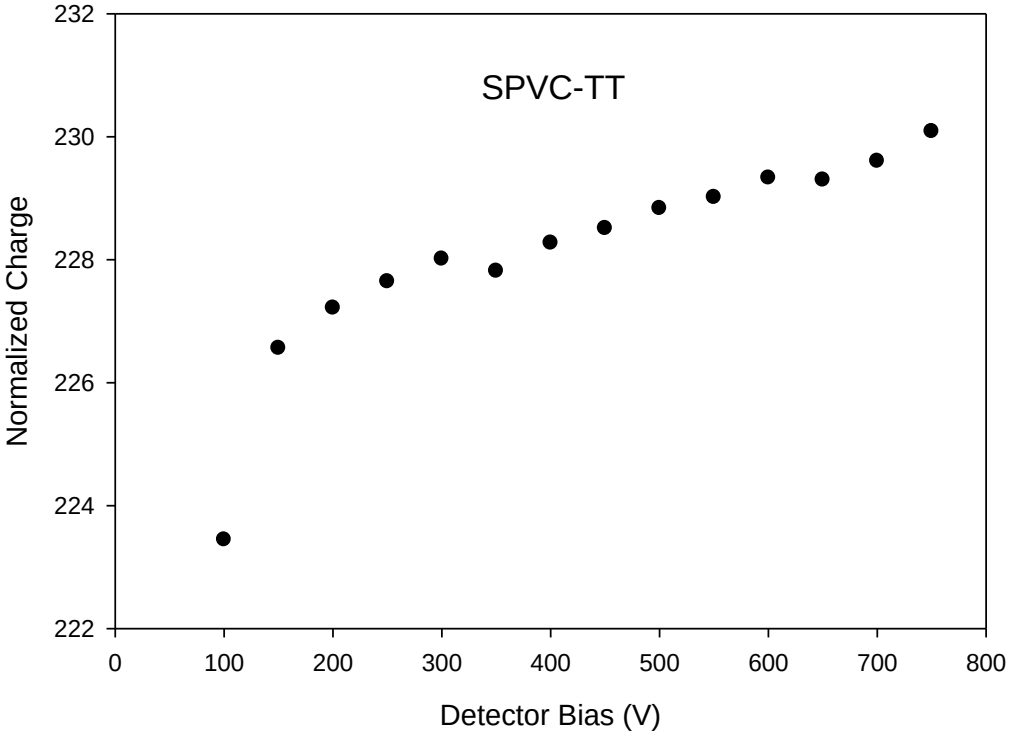

Figure B.6 - Operating voltage trials for the SPVC-NR detector.

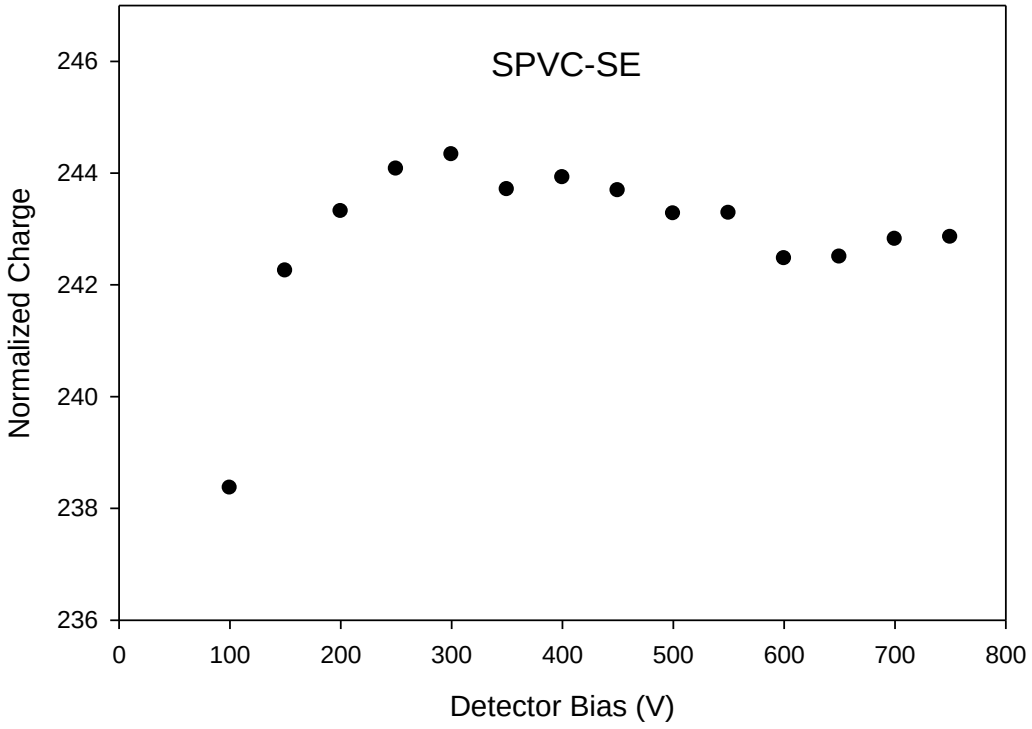

Figure B.7 - Operating voltage trials for the SPVC-SE detecto

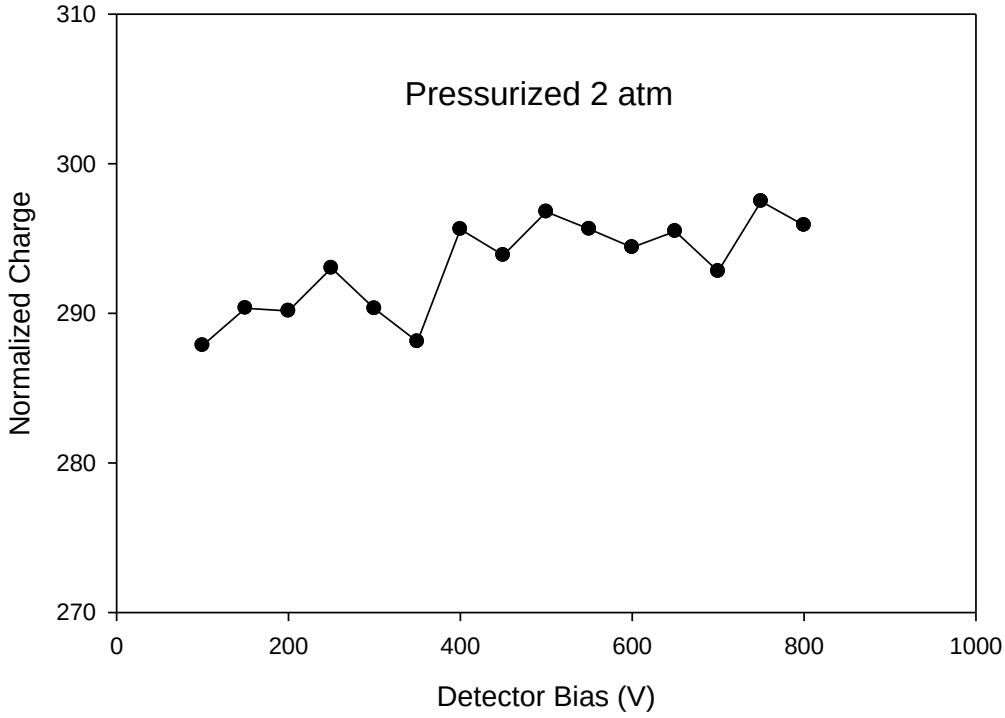

Figure B.8 - Operating voltage trials for the pressurized detector at 2 atm.

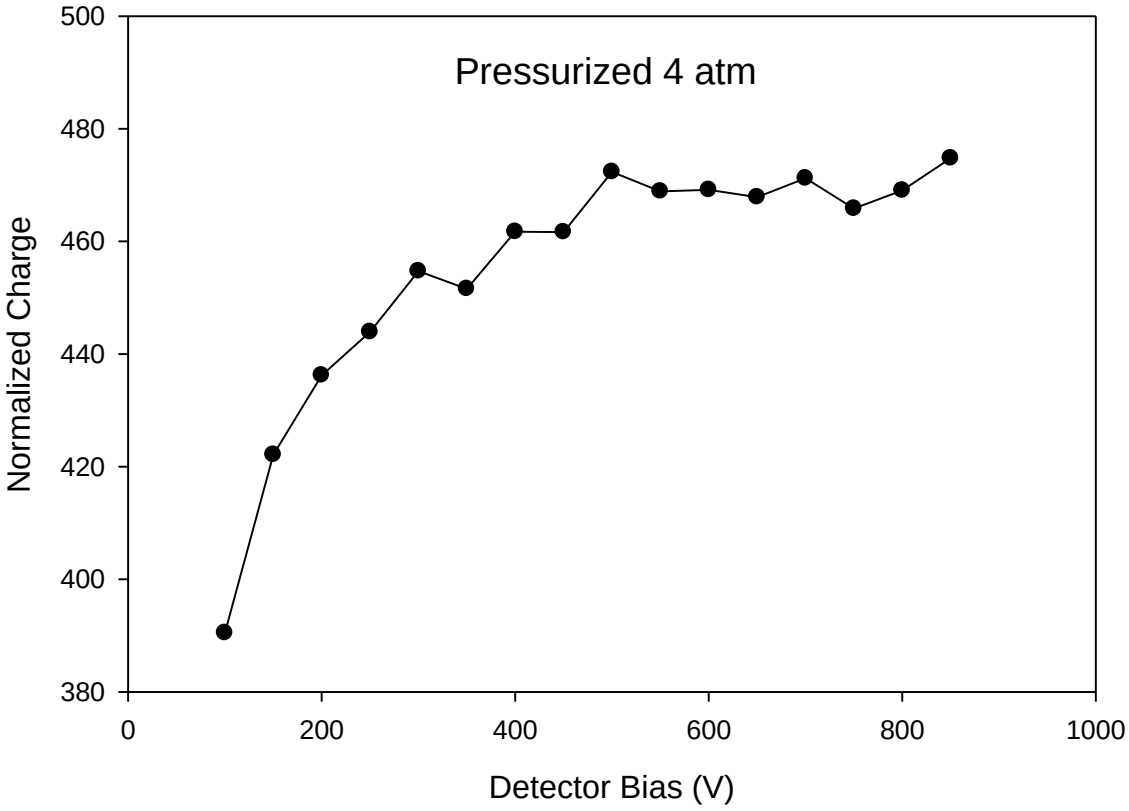

Figure B.9 - Operating voltage trials for the pressurized detector at 4 atm.

VITA

Joseph Ross

Candidate for the Degree of

Master of Science

Thesis: DESIGN OF IONIZATION CHAMBERS FOR USE TEACHING X-RAY DOSIMETRY

Major Field: Physics

Biographical:

Education:

Completed the requirements for the Master of Science in Physics at Oklahoma State University, Stillwater, Oklahoma in July, 2015.

Completed the requirements for the Bachelor of Science in Medical Physics at East Central University, Ada, Oklahoma in December 2009.